Proceedings of the Geologists' Association 124 (2013) 834–854

Contents lists available at SciVerse ScienceDirect

Proceedings of the Geologists' Association

journal homepage: www.elsevier.com/locate/pgeola

New insights into the deformation of a Middle Pleistocene glaciotectonised sequence in Norfolk, England through magnetic and structural analysis

Edward J. Fleming [a,b,*], Carl T.E. Stevenson [a], Michael S. Petronis [c]

[a] School of Geography, Earth and Environmental sciences, University of Birmingham, B15 2TT, UK
[b] Department of Arctic Geology, The University Centre in Svalbard (UNIS), P.O. Box 15, N-9171 Longyearbyen, Norway
[c] Environmental Geology, Natural Resource Management Department, New Mexico Highlands University, Las Vegas, NM 87701, USA

ARTICLE INFO

Article history:
Received 25 May 2012
Received in revised form 2 November 2012
Accepted 19 November 2012
Available online 21 December 2012

Keywords:
Anisotropy of magnetic susceptibility (AMS)
Glaciotectonism
Norfolk
Sheath folding
Quaternary
Strain

ABSTRACT

North Norfolk is a classic area for the study of glacial sediments with a complex glaciotectonic deformational history, but the processes leading to the formation of some structures can be ambiguous. Anisotropy of magnetic susceptibility (AMS) analyses, providing quantitative fabric data, have been combined with the analysis of visible structures and applied to the Bacton Green Till Member, exposed at Bacton, Norfolk. Thermomagnetic curves, low temperature susceptibility and acquisition of isothermal remanent magnetism (IRM) reveal that the magnetic mineralogy is dominated by paramagnetic phases. The magnetic foliation is parallel to fold axial planes and weakly inclined to bedding, whilst the magnetic lineation is orientated parallel to stretching, indicated by the presence of stretching lineations and the trend of sheath folds. Variations in the orientation of the magnetic lineation suggest that the Bacton section has been subject to polyphase deformation. After subaqueous deposition, the sequence was overridden by ice and glaciotectonically deformed which involved stretching initially north–south, then east–west. These results show that AMS can be used to detect strain in three dimensions through a glaciotectonite where paramagnetic mineralogy is dominant. This approach therefore provides further support to the use of AMS as a fast, objective and accurate method of examining strain within deformed glacial sediments.

1. Introduction

In this paper we demonstrate the power of an under-utilised geophysical technique for determining the fabric of dynamically deposited glacial deposits and the directions of the flows that created them. The role of deformable materials beneath glaciers is currently one of the most important topics in glaciology, and various authors have suggested that glacier motion is facilitated by shearing of the glacier bed (e.g., Alley et al., 1986, 1987; Boulton, 1986). Sub-sole deformation is considered to be the primary mechanism for sustaining fast flow in ice streams and outlet glaciers and is therefore of great importance for investigations into ice sheet stability (Clark, 1994; MacAyeal, 1992). Deformation of the bed has been successfully measured in several cases (e.g., Boulton et al., 2001; Boulton and Hindmarsh, 1987; Hart et al., 2011; Iverson et al., 2003); however, the study of basal conditions in active glaciers is challenging because of the inaccessibility of the bed and the short length of time over which data can be recorded. Instead, the primary evidence used to infer dynamic processes has been through the properties of the glacigenic sediments and landforms left behind by the large ice sheets that covered much of North America and Europe during the Pleistocene Epoch (Licciardi et al., 1998; Piotrowski et al., 2001).

Glaciotectonism is the structural deformation of the upper horizon of the lithosphere by glacial stresses (Slater, 1926; van der Wateren, 2002). Glacially deformed sediment is often referred to as a glaciotectonite, a term first introduced by Banham (1977) to describe penetrative, subglacially sheared sediments analogous to mylonites in metamorphic rocks. In most studies, a wider definition is used to encompass a body of unlithified or weakly lithified sediment deformed by glacial stresses (Benn and Evans, 2010; van der Wateren, 2002). Within such sediments, distinct structures form such as folds, faults, boudins and fabrics (Hart and Rose, 2001). These structures can be analysed on both macroscopic scales (e.g., Benediktsson et al., 2010; Hart, 1990; Hart and Boulton, 1991; Lee and Phillips, 2008; Lesemann et al., 2010) and microscopic scales (e.g., Menzies et al., 2006; Phillips and Auton, 2000; Phillips et al., 2007, 2011; van der Meer, 1993; van der Wateren et al., 2000) and can provide considerable information about the genetic environment and deformational history. For example, in a subglacial environment, deformation is typically

* Corresponding author at: School of Geography, Earth and Environmental sciences, University of Birmingham, B15 2TT, UK. Tel.: +44 01214 146165.
E-mail address: ejf011@bham.ac.uk (E.J. Fleming).

0016-7878
http://dx.doi.org/10.1016/j.pgeola.2012.11.004

dominated by simple shear coupled with extreme extension (Hart and Boulton, 1991; Kluiving et al., 1991), whilst in proglacial settings, glaciotectonic compression may facilitate the formation of structures analogous to fold and thrust belts in an orogenic foreland setting (Bennett, 2001; Hambrey et al., 1997; Huddart and Hambrey, 1996; Phillips et al., 2008). Similar structures, however, can be seen in both settings and may not be readily distinguishable (Phillips et al., 2007). Variation in lithology and the dynamic nature of subglacial conditions means that earlier deformation structures can be overprinted (Evans and Hiemstra, 2005; Piotrowski et al., 2004). Moreover, fold structures, similar to those found in glaciotectonic environments, are also found in other environments, e.g. slumping on glaciomarine slopes (Arnaud and Eyles, 2002; Eyles and Kocsis, 1988; Kurtz and Anderson, 1979). This makes the interpretation of specific structures ambiguous, and in some stratigraphic sections the same evidence has been interpreted as being formed by very different processes. For example, the soft sediment deformational structures in the 'North Sea Drifts' of Norfolk, UK, are traditionally interpreted as subglacial (Banham, 1975) but have also been reinterpreted as slumping in a glaciomarine setting (Eyles et al., 1989). The objectivity and usefulness of certain techniques used to study subglacial deformation has been doubted (Bennett et al., 1999; Zaniewski and van der Meer, 2005), and it is apparent that there is a clear need for objective and quantitative approaches to the analysis of strain within glacial sediments.

In North Norfolk, England, although exposures provide classic sections from which original work on glaciotectonics emerged (Banham, 1977, 1988; Banham and Ranson, 1965; Slater, 1926), considerable debate remains over the pattern of lowland glaciation (Banham et al., 2001; Eyles et al., 1989; Gibbard and Clark, 2011; Hamblin et al., 2005). Here, we reinvestigate sediment genesis and flow vectors using the analysis of the anisotropy of magnetic susceptibility (AMS) technique. The AMS technique is widely used in structural geology but has seldom been used in glacial geology until recently. Fuller (1962), through comparisons with pebble fabrics, was the first to suggest that magnetic fabrics could be a viable technique for petrofabric analysis. The magnetic properties of till sequences in North America, relating to the Laurentide ice sheet, have since been investigated (Eyles et al., 1987; Gentoso et al., 2012; Stewart et al., 1988; Stupavsky and Gravenor, 1975; Stupavsky et al., 1974a,b). Recent laboratory work (Hooyer et al., 2008; Thomason and Iverson, 2006) has increased confidence in the reliability of the technique as a quick and objective method of examining strain within deformed sediments.

2. The development and interpretation of AMS fabrics in glacial sediments

When subjected to an external magnetic field, an induced magnetism is generated in a rock or sediment that is dependent on the magnetic susceptibility. This can be represented by the equation $M = KH$, where M is the induced magnetisation, H is the applied field and K is the magnetic susceptibility (Tarling and Hrouda, 1993). Variation in K with direction can be visualised by a second rank symmetrical tensor through the maximum (K_1), intermediate (K_2) and minimum (K_3) principal susceptibility axes. The orientation of the susceptibility axes is controlled by the alignment, distribution and crystalline properties of magnetic minerals; thus AMS can be used to detect very weak or subtle fabrics.

In a subaqueous environment, the alignment of minerals is controlled by gravitational and hydrodynamic processes (Tarling and Hrouda, 1993). When deposition occurs in still water, gravitational settling is the only significant force and causes platy grains to become aligned parallel to the depositional surface, giving rise to a strongly oblate fabric confined to the bedding plane. The notable exception to this is fine-grained ferromagnetic grains, which can become aligned parallel to the Earth's magnetic field. If hydrodynamic disruption occurs, i.e. from currents acting on the sea floor, then the long axis of grains can rotate and become preferentially aligned, and lineations can develop reflecting flow directions (Rees and Woodall, 1975). Post-depositional, soft-sediment processes can also have a significant impact on such primary depositional fabrics (Schwehr and Tauxe, 2003). Stress acting on the sediment can cause grains to rotate resulting in the preferential alignment of their long axes to shear direction and short axes perpendicular to the shear plane. In this way, AMS has been used to resolve strain that is difficult to detect using other petrofabric techniques (Borradaile and Tarling, 1981; Cifelli et al., 2009; Kissel et al., 1986; Mattei et al., 1997).

Previous work that has been carried out on the AMS of glacial sediments has largely focussed on determining ice flow directions and bed dynamics from fabrics within tills (Shumway and Iverson, 2009; Thomason and Iverson, 2009), and flow directions from mass flow units (Archanjo et al., 2006; Eyles et al., 1987). In a subglacial environment, Iverson et al. (2008) showed through ring shear experiments that when an intact till sample was sheared under conditions similar to those expected to operate at the bed, microfaults develop that facilitate the rotation of the long axis of particles into the plane of shear, where they remain. This evidence was used to support the idea of *March-type rotation* (March, 1932), where behaviour is consistent with Coulomb-plastic rheology, as opposed to *Jeffery-type rotation* (Jeffery, 1922), where particles can roll continuously in a shearing viscous medium (Benn, 1995; Thomason and Iverson, 2006). No published data, however, exist for the measurement of cumulative strain through AMS within glaciotectonites, where pre-existing unconsolidated sediment has been glacially deformed such that relicts of the original structures remain.

3. Geological background

The bedrock geology of North Norfolk consists of gently dipping Cretaceous chalk. Pleistocene aged sediments consisting of pre-glacial fluvial and shallow marine deposits overlie the Cretaceous chalk, which in turn are overlain by a sequence of tills separated by outwash sediments (Banham, 1968). These glacial sediments were previously considered to have been deposited by oscillations at the margins of coexisting British and Scandinavian ice sheets during the Anglian glaciation (478–424 Ka, Marine Isotope Stage 12) (Bowen et al., 1986; Fish and Whiteman, 2001; Lunkka, 1994; Perrin et al., 1979). A new glacial lithostratigraphy has been proposed (Hamblin, 2000; Hamblin et al., 2005; Lee et al., 2004; Rose et al., 2001), subdividing the sequence into four formations; the Happisburgh, Lowestoft, Sheringham Cliffs and Briton's Lane. These authors suggested that the deposition of the tills were associated with an entirely British-based, as opposed to Scandinavian, ice sheet (Hamblin et al., 2005; Lee et al., 2002). This interpretation has been disputed (Banham et al., 2001; Gibbard and Clark, 2011; Preece et al., 2009) because of its inability to explain biostratigraphical evidence.

The study site in North Norfolk is located in a cliff section near the village of Bacton (National Grid Reference TG 338345; Fig. 1). The lithology consists of a stratified diamicton sequence, previously referred to as the 3rd Cromer Till (Banham, 1968; Lunkka, 1994) but reassigned to the Bacton Green Till Member of the Sheringham Cliffs Formation (Hamblin et al., 2005; Lee and Phillips, 2008) through tectono-stratigraphic relationships and petrological analyses. Although not directly exposed at the section, further along the coastline, the Bacton Green Till Member overlies the Walcott Till member, previously referred to as the 2nd Cromer

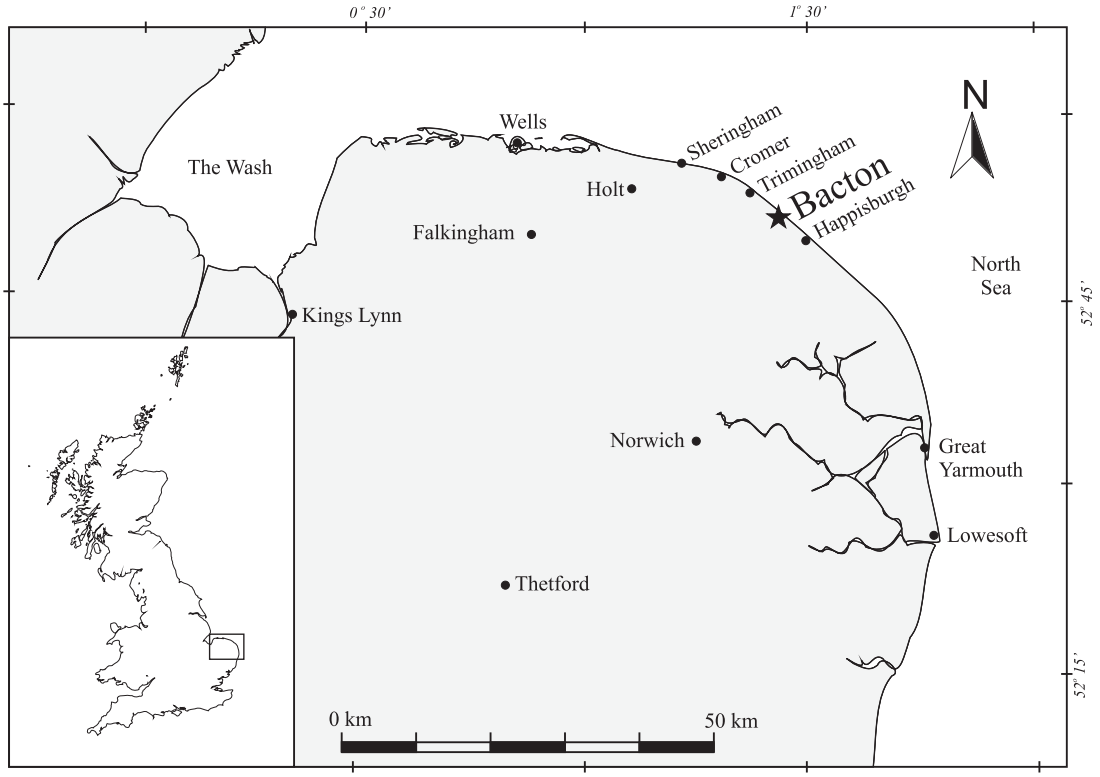

Fig. 1. Map of the Norfolk coastline showing the location of Bacton (Black Star), National Grid Reference TG 338345.

Till (Banham, 1968; Lunkka, 1994) and an interglacial, fluviodeltaic, glacial outwash sand, assigned to the Mundesley Sand Member. The top of the Bacton Green Till Member is truncated by the Stow Hill Sand and Gravel Member of the Britons Lane Formation.

The Bacton Green Till Member consists of a massive to weakly laminated, grey to brown coloured sandy diamicton with horizons of sand and gravel (Fig. 2) and Bacton is considered the type location for the member (Hamblin et al., 2005). Initial deposition has been suggested to have occurred in a subaqueous setting through processes of mass flow, turbidity currents and rapid rainout, associated with an ice advance from the north (Lee and Phillips, 2008; Lunkka, 1994; Phillips et al., 2008). For simplicity, we adopt the terminology previously used at the site and continue to refer to the Bacton Green Till Member, whilst acknowledging the subtly different definition of a till *sensu stricto* (cf. Benn and Evans, 2010) as this evokes deposition directly from glacier ice, which is not considered the case for the Bacton Green Till Member (Hamblin et al., 2005; Lee and Phillips, 2008; Lunkka, 1994).

Previous authors have suggested that, after deposition, the Bacton Green Till Member was glaciotectonically deformed creating the structures observed, associated with an ice advance from the west or southwest (Lee and Phillips, 2008; Phillips et al., 2008; Scheib et al., 2011). Regional ice flow directions across the region, however, are equivocal (cf. Hamblin et al., 2005), and many of the structures seen could arguably have been formed in an entirely subaqueous setting without the need for glaciotectonic deformation (Eyles et al., 1989).

At the Bacton locality, Lee and Phillips (2008) concluded that the sequence had been affected by three phases of glaciotectonic deformation. Phase 1 was characterised by ductile deformation through northward-verging isoclinal recumbent folds. During Phase 2, conditions switched to a non-dilated state, leading to brittle deformation through subhorizontal, north-verging thrusts, and Riedel shears. Slices of the underlying Mundesley Sand Member were thrust into the Bacton Green Till member, forming sand lenses interpreted as augens. Phase 3 deformation resulted in the formation of sand-filled fractures, interpreted as hydrofractures, through water escape from a confined aquifer. It was interpreted that these north-orientated structures were all associated with an ice advance from the southwest, loosely fitting in with a regional model which predicted ice flow from the west or southwest (Fish and Whiteman, 2001; Perrin et al., 1979; Scheib et al., 2011; West and Donner, 1956). In contrast, other investigations of the Bacton Green Till Member, from other localities, have found that the unit exhibits a phase of deformation from the northwest based on geomorphology, pebble fabrics and macroscopic structures (Hart, 2007) and there is clearly still a lack of consensus into the pattern of ice flow across the region.

4. Methods

For the analysis of AMS, 21 sample sites were chosen covering both lateral and vertical changes within the succession (location shown in Fig. 5). The sampled lithologies were mostly diamicton or sandy diamicton, classified using the Hambrey and Glasser (2003) modification of Moncrieff (1989). To avoid sampling-induced anisotropy, the adopted method involved excavating back 20 cm into the cliff face to remove any effects of surface disruption. Blocks of approximately 20 cm × 10 cm × 10 cm were orientated using a Brunton compass, cut out of the exposed surface and labelled BG1–BG21. These blocks were subsequently air-dried over a period of 1 week, impregnated with a sodium silicate solution followed by an epoxy resin and cut using a diamond-tipped rock saw into 2-cm sided cubic subsamples for AMS measurement.

AMS measurements were carried out using an AGICO KLY-3 Kappabridge at the University of Birmingham. In total, 324 cubes were measured with an average of 19 samples per site. The following parameters were used to evaluate the susceptibility

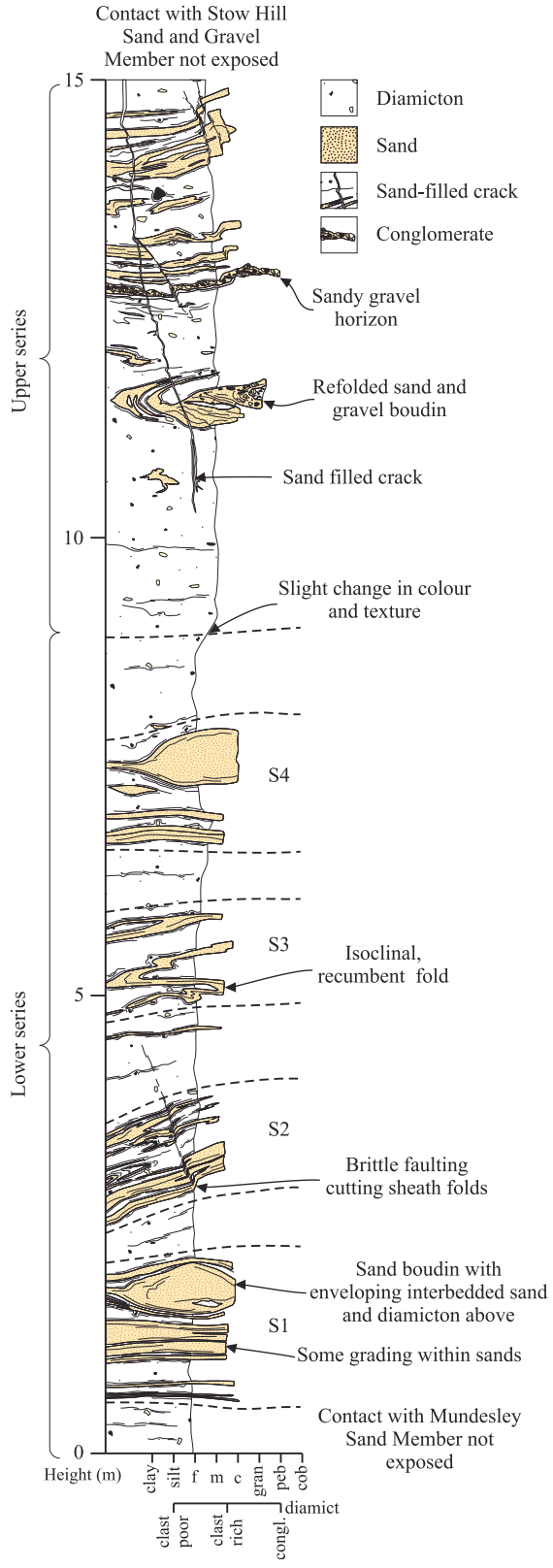

Fig. 2. Sedimentary log through the section at the study site, divided into upper and lower series based on style of deformation structures and distribution of magnetic fabrics. S1–S4 refers to horizons with sandy layers and sand lenses. A sand-filled crack is shown at the top cutting across deformation structures and bedding.

ellipsoid (cf. Tarling and Hrouda, 1993). The mean susceptibility (K_{mean}) is given by

$$K_{mean} = \frac{(K_1 + K_2 + K_3)}{3},$$

where ($K_1 > K_2 > K_3$) are the principal susceptibilities (SI units). The shape of the ellipsoid can be characterised using lineation (L) and foliation (F) parameters (Khan, 1962) and are calculated as:

$$L = \frac{(K_1 - K_2)}{K_{mean}}$$

and

$$F = \frac{(K_2 - K_3)}{K_{mean}}$$

Also used are the corrected anisotropy degree (P_j), to determine the strength of the fabric, and the shape parameter (T), to calculate the shape of the susceptibility ellipsoid (Jelínek, 1981), which, respectively, are:

$$P_j = \exp\left(\sqrt{2\left[\left(\ln\left(\frac{K_1}{K_3}\right)\right)^2 + \left(\ln\left(\frac{K_1}{K}\right)\right)\right]}\right)$$

and

$$T = \lfloor \frac{2\ln(K_2/K_3)}{\ln(K_2/K_3)} \rfloor - 1.$$

In order to interpret the magnetic fabrics, the magnetic mineralogy must be identified, as sediment composed of different magnetic minerals (e.g., magnetite, haematite, titanomaghaemite and pyrrhotite) will produce very different fabric characteristics. In addition to the composition of the Fe-oxides, magnetic grain shape and grain size, which controls domain state, play an integral role in defining the magnetic fabric of a material. Equidimensional magnetite grains lack shape anisotropy and are nearly magnetically isotropic in weak applied fields. The grain size of the magnetic grains is of particular importance in the study of magnetic fabrics as, depending on grain size, the orientation of the maximum and minimum susceptibility axes can be inverted (Tarling and Hrouda, 1993). As grain size increases, the magnetic domain state changes from single-domain (~0.07 μm) to multi-domain. The anisotropy of single-domain grains produces a magnetic fabric that is opposite to that of multi-domain grains. The maximum susceptibility of large, multi-domain grains is parallel to their long axes, while in single domain grains the maximum susceptibility axes are perpendicular to the long axis. This arises because a single-domain grain cannot be magnetised along its long axis by a weak applied field, so it essentially has zero susceptibility along that axis and a maximum susceptibility along its short axis (Tarling and Hrouda, 1993). Sediment overwhelmingly dominated by single-domain magnetite can produce what is known as an "inverse magnetic fabric". Identifying the magnetic mineralogy is thus critical when interpreting magnetic fabrics. For example, if fabric carried by single-domain grains is interpreted as a "normal magnetic fabric" it would lead to an erroneous interpretation essentially perpendicular to the true fabric orientation.

Investigations of the magnetic mineralogy were conducted at the New Mexico Highlands University (NMHU) Paleomagnetic and Rock Magnetism Laboratory. Thermomagnetic experiments were conducted for all 21 samples from room temperature (21 °C) to 700 °C using the AGICO MFK-1A Kappabridge with a CS4 high temperature susceptibility attachment. AF-demagnetisation of the natural remanent magnetisation (NRM) experiments were conducted by exposing the sample to an alternating magnetic field in a progressive

stepwise manner up to a 120 mT peak applied field. Acquisition of isothermal remanent magnetisation (IRM) experiments (i.e., partial hysteresis loops) were carried out for six samples by inducing an external applied field, at progressive stronger applied fields up to a peak of 2.5 T. Both the AF-demagnetisation and partial hysteresis loops were measured on an AGICO JR6-A dual-speed spinner magnetometer, in a magnetically shielded room that attenuates Earth's field to less than 0.1%. Low-temperature susceptibility experiments were conducted on all sites using an in-house built cryostat system coupled with the MFK-1A Kappabridge. The samples were cooled to 77 K in liquid nitrogen, and the bulk susceptibility measured every 18 s during warming to room temperature.

Thin sections were prepared of samples BG3, BG13, BG16 and BG21. These were impregnated with an epoxy resin, cut and polished using standard procedures and examined under polarised transmitted light.

Structural data was collected in the field. The unconsolidated nature of the diamicton provided access to a three-dimensional view through excavation. Linear data (fold axes and stretching lineations) were measured as plunge and trend, whilst planar data (bedding, faults, fold axial planes and sand-filled cracks) were measured as strike and dip. The contacts around sand lenses were measured and the trends of the lenses were calculated by the fit of great circles to the poles.

5. Results

5.1. Magnetic mineralogy

The mean susceptibility (K_{mean}) (Table 1; see Section 4 for derivation) of the samples range from 0.05 to 0.27 $\times$ 10^{-3} (average 0.13 $\times$ 10^{-3}) (in the SI system), and the corrected degree of anisotropy (P_j) varies between 1.007 and 1.09 (average 1.033). These values indicate that the paramagnetic fraction provides a major contribution to the susceptibility with little contribution by ferromagnetic phases (Borradaile and Henry, 1997; Rochette, 1987). Low-temperature susceptibility (Fig. 3c) experiments yield a temperature-dependent behaviour on heating from 77 to 295 K as predicted by the Curie–Weiss law of paramagnetic materials (Nagata, 1961; Richter and van der Pluijm, 1994). Antiferromagnetic, diamagnetic and ferromagnetic materials yield a temperature-independent susceptibility in the range used in the low-temperature experiments (77–295 K). These results indicate that paramagnetic minerals are controlling the susceptibility and the anisotropy of the sediments.

The variation of low-field susceptibility with temperature was also used to investigate the magnetic mineralogy (Fig. 3a). Curie-point estimates and phase transitions of magnetic minerals may be identified from the resultant plot. Low-field susceptibilities remain constant or decrease smoothly up to 400 °C, after which susceptibilities increase before decreasing rapidly above 550 °C. Cooling curves are irreversible, showing a strong increase in magnetic susceptibility. This pattern suggests the formation of secondary magnetic phases at temperatures above 400 °C, but this may also be due to a minor amount of single-domain magnetite being present within the samples that results in a suppressed Hopkinson Peak near the Curie point of low Ti-titanomagnetite (Dunlop and Ozdemir, 1997; Hopkinson, 1890).

To better constrain the magnetic mineralogy, AF-demagnetisation of the NRM (Fig. 3b) and the acquisition of IRM experiments (Fig. 3d) were performed. AF-demagnetisation can be used to discriminate between single-domain and multi-domain magnetite. Single-domain grains have a higher medium destructive field (MDF) than multi-domain grains. IRM acquisition experiments can distinguish the composition of magnetic minerals. For example, the saturation magnetisation of haematite is near 3 T whilst magnetite is fully saturated by 300 mT. Of the 6 sites examined, 3 sites, all from the lower series (Fig. 5), responded well to AF-demagnetisation and yield a MDF of 50–60 mT (Fig. 3b). This indicates that a high-coercivity phase, probably single-domain magnetite, is present carrying the remanent magnetism (Dunlop and Ozdemir, 1997). Sites BG20 and BG21 from the upper series (Fig. 5) and from the sand lens (BG14) did not respond to AF-demagnetisation indicating that a magnetically hard phase is present. Similarly, IRM acquisition curves are typically steep, indicating the presence of a low coercivity phase (e.g. low Ti-titanomagnetite), yet most samples do not reach saturation until after 2.5 T (Fig. 3d), suggesting the presence of another high coercivity phase (presumably haematite).

In thin section, the samples are composed of a range of clasts in a clay-silt matrix. Clasts are predominantly quartz with a small proportion of shell fragments and other lithics. They are typically granule- to sand-sized, angular to rounded and have no apparent preferred alignment of long axes. Haematite grains are present, but other opaque minerals are rare. Pigmentary haematite is sometimes

Table 1
Mean site AMS data for the Bacton Green Till Member (see Section 3 for calculation): N, number of samples; K_m, mean susceptibility; K_1, K_2, K_3, orientations (declination and inclination) of the principal susceptibility axes with 95% confidence ellipses; L, lineation ($L = K_1/K_2$); F, foliation ($F = K_2/K_3$); P_j, anisotropy degree; T, shape parameter; and height (m), stratigraphic height above base at which the sample was taken.

Site	N	$K_m \times 10^{-3}$	K_1	K_1 95% error	K_2	K_2 95% error	K_3	K_3 95% error	L	F	P_j	T	Height (m)
BG1	19	0.135	171/5	42/4	79/21	42/6	273/68	7/4	1.036	1.039	1.047	0.878	3.3
BG2	19	0.192	354/48	22/4	86/23	22/4	253/64	4/4	1.005	1.025	1.032	0.680	3.6
BG3	19	0.191	117/1	26/5	26/20	26/8	211/71	9/5	1.004	1.021	1.027	0.700	3.1
BG4	20	0.113	333/26	52/5	243/1	52/7	125/87	7/5	1.002	1.025	1.031	0.856	3.6
BG5	18	0.101	243/0	35/4	333/12	36/6	151/78	11/4	1.002	1.009	1.012	0.582	5.4
BG6	18	0.133	91/20	27/4	358/8	27/3	248/69	4/3	1.004	1.037	1.046	0.781	2.1
BG7	15	0.267	335/8	15/4	245/4	15/4	129/82	4/4	1.008	1.025	1.034	0.517	5.5
BG8	20	0.015	212/8	64/28	304/16	64/19	94/72	28/20	1.001	1.006	1.007	0.723	12.6
BG9	20	0.073	96/2	25/14	6/4	25/23	211/86	24/12	1.004	1.005	1.009	0.130	13.4
BG10	20	0.119	281/7	32/6	191/1	32/6	94/83	7/6	1.004	1.018	1.024	0.599	14.1
BG11	17	0.071	86/7	32/9	355/13	31/12	202/75	14/9	1.003	1.011	1.015	0.567	11.0
BG12	16	0.077	96/2	28/9	6/4	28/16	209/86	17/9	1.003	1.008	1.012	0.421	9.2
BG13	20	0.166	355/19	28/3	94/26	28/3	233/57	4/3	1.004	1.035	1.043	0.798	2.4
BG14	15	0.104	29/25	13/5	120/1	13/4	212/65	6/4	1.026	1.060	1.090	0.384	3.0
BG15	20	0.145	0/2	25/5	91/31	25/5	268/59	6/5	1.006	1.024	1.032	0.622	2.2
BG16	28	0.166	35/4	41/5	126/22	41/7	295/68	7/5	1.002	1.027	1.033	0.833	6.3
BG17	18	0.107	358/2	30/5	90/34	30/9	265/56	11/6	1.007	1.036	1.047	0.673	6.2
BG18	20	0.130	162/7	8/4	252/1	11/8	353/83	11/4	1.018	1.024	1.043	0.153	6.4
BG19	20	0.055	68/52	24/12	335/2	40/16	243/38	37/13	1.019	1.025	1.044	0.134	10.9
BG20	20	0.119	254/37	32/6	157/10	32/6	54/51	7/6	1.004	1.018	1.024	0.599	11.9
BG21	19	0.061	248/5	27/15	157/4	24/15	27/84	26/5	1.010	1.024	1.035	0.407	14.8

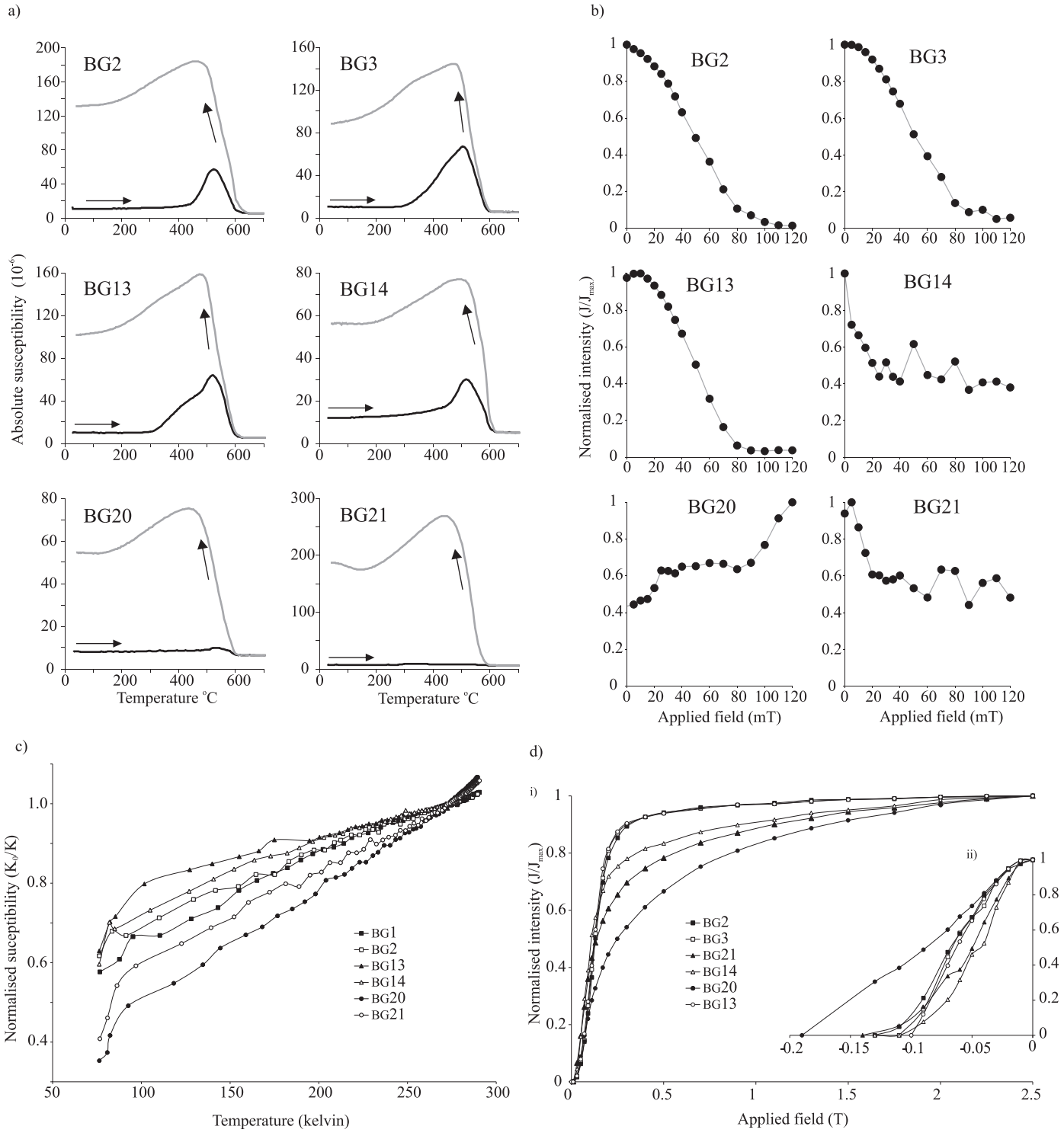

Fig. 3. Rock magnetic experiments. (a) Low-field susceptibility (K) vs. temperature curves. In each case, the heating curve is black and the cooling curve is grey. (b) AF-demagnetisation curves with the normalised magnetisation intensity (M/Max) plotted against the demagnetising field (mT). Samples BG2, BG3 and BG14 reveal a well defined characteristic remanent magnetism that decays to the origin with average medium destructive fields at 50–60 mT. Samples BG14, BG20 and BG21 do not respond to AF-demagnetisation. (c) Temperature vs. the normalised reciprocal (K/Ko) susceptibility. Paramagnetic susceptibility is a function of temperature and follows the Curie–Weiss law ($K_p = C/(T - \theta)$) with C = Curie constant, T is temperature, and θ is the paramagnetic Curie temperature. The K/K_o transforms a paramagnetic curve into a straight line, with an intercept that defines the paramagnetic Curie temperature. Ferromagnetic materials have no susceptibility dependence above the Verway transition (~120 K) and plots as a straight line of zero slope. (d) Normalised (J/J_{max}) acquisition of isothermal remanent magnetisation (IRM) experiments with (i) IRM acquisition and (ii) Backfield IRM acquisition. See Fig. 5 for sample locations.

observed obscuring a clay-rich matrix. The paramagnetic fraction largely controlling the AMS is therefore likely to be within this matrix which, based on X-ray diffraction (XRD) analysis of the North Norfolk tills, is likely to be a combination of chlorite, kaolinite and illite (Kazi, 1972).

5.2. Anisotropy of magnetic susceptibility

All samples yield susceptibility ellipsoids where $F > L$ (i.e. dominantly oblate) (Table 1 and graphically represented in Fig. 4a and b). The corrected degree of anisotropy (P_j) vs. mean

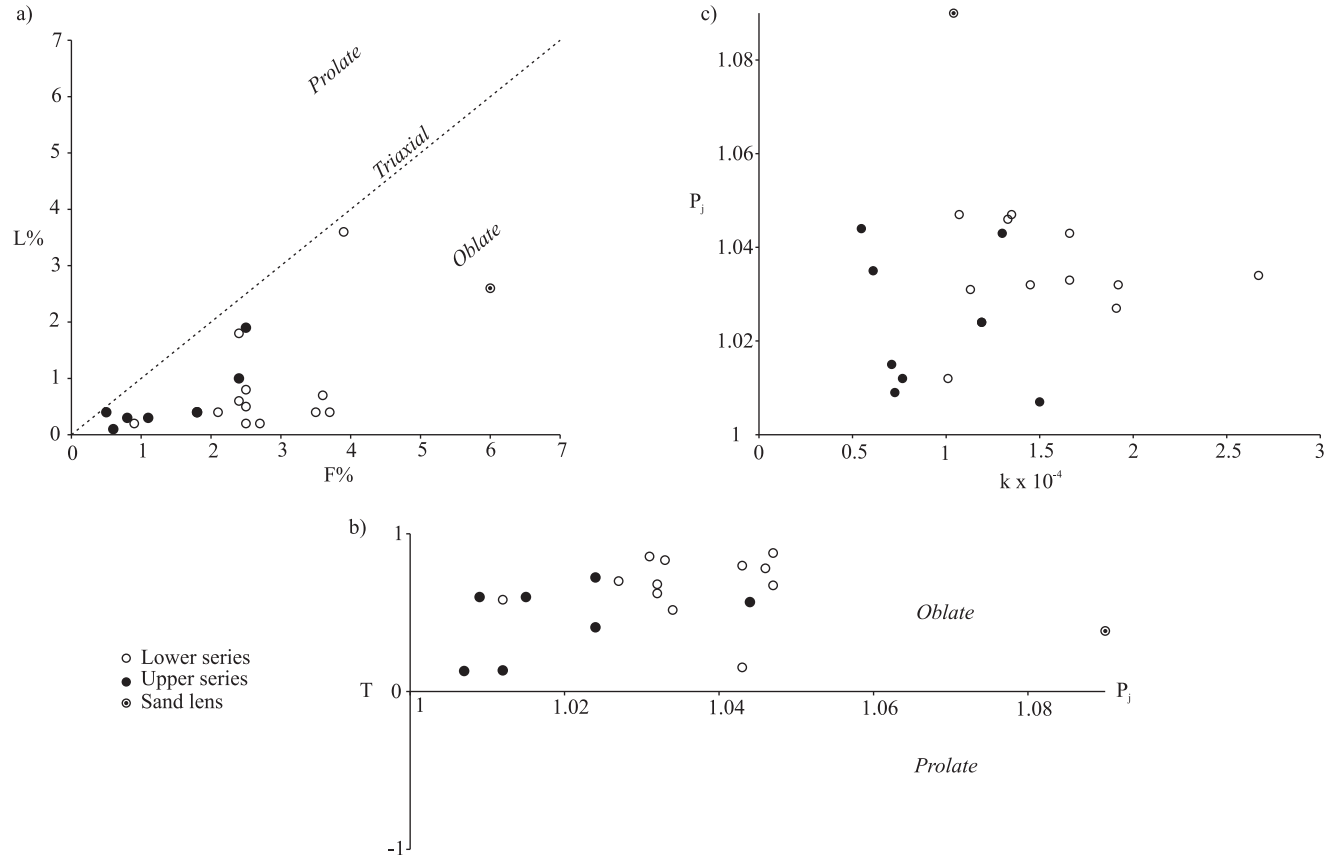

Fig. 4. Variation of AMS parameters for all samples showing upper series (black circles), lower series (white circles) and sand lens (black and white circles). (a) *L%* vs. *F%* (magnetic lineation vs. magnetic foliation). (b) Shape parameter (*T*) vs. anisotropy parameter (P_j). (c) Anisotropy parameter (P_j) vs. susceptibility (*K*).

susceptibility (K_m) is shown in Fig. 4c and reveals that the shape of the fabric is not dependent on the strength of susceptibility, which may be the case if different magnetic mineral phases, were controlling the susceptibility at different sites. Fig. 4a shows a graphic display of magnetic lineations (*L%*) vs. magnetic foliation (*F%*). Strongly prolate ellipsoids lie near the *L* axis and strongly oblate ellipsoids lie near the *F* axis with triaxial fabrics occurring near the centre of the diagram. Also shown (Fig. 4b) are the conventionally used T/P_j plots which show an alternative, albeit criticised (Borradaile and Jackson, 2004), method of displaying ellipsoid shape. In both plots, ellipsoids are within the oblate to triaxial realm.

Lower hemisphere stereographic projections of the AMS results, with spatial references to the site at which the sample was taken, are shown in Fig. 5. The minimum susceptibility axes (K_3) are perpendicular to the bedding, defined by the $K_1 - K_2$ plane. K_3 is mostly steeply plunging to vertical, showing a gently dipping magnetic foliation of variable strike. Magnetic lineations are defined by the K_1 axes, which reveal a clear separation between the upper and lower series. In the lower series, the majority of magnetic lineations trend north–south with mean magnetic lineations clustering at 002° and plunging 6° (Fig. 6a), whilst in the upper series there is a switch in trend to east–west and mean magnetic lineations cluster at 267° and plunging 6° (Fig. 6b).

5.3. Visible structures

Post-depositional deformation has affected the original sedimentary lamination producing a variety of structures. These can be analysed using standard structural techniques and can be used to compare strain directions with those calculated from magnetic fabrics. Deformation has taken place in both brittle- and ductile-like manners. The term ductile is used to refer to structures resulting in permanent, continuous deformation, without fractures seen at the outcrop scale and brittle to refer to structures at which deformation is isolated to narrow shear zones, between blocks. There is a vertical change in the styles of deformation as is seen in the magnetic fabrics, and as a result, they are divided into the upper and lower series accordingly.

5.3.1. Folding and limb attenuation

Folding and boudinage is common throughout the section (Figs. 7–9). Within the lower series, the original sedimentary layering of the stratified diamicton has been strongly attenuated resulting in laterally discontinuous "stringers" of sand (Fig. 7b). These stringers typically lie in a north–south orientation and are folded in places (e.g. Fig. 7a). Folds are typically steeply inclined to recumbent and asymmetric, with inter-limb angles ranging from tight to isoclinal. Vergence of these folds seems to be in both directions (Fig. 7c), a characteristic typical of sheath folding (Alsop and Holdsworth, 2004; Kluiving et al., 1991). The axes of these sheath folds are typically moderately to highly curvilinear with axial planes parallel to subparallel to the stratification. Measurements of fold axes (Fig. 9a) show a range of orientations with a distinct clustering plunging 16° to 016°. This orientation is subparallel to the mean lineations of the magnetic fabrics in the lower series (Figs. 5a and 6).

Within the upper series (Fig. 11), the boudinage of more competent sandy horizons has also resulted in sand stringers and folding is common. Folds are typically moderately inclined to recumbent with interlimb angles ranging from close to isoclinal. Folding styles are more irregular and axial planes cannot be traced throughout the section. The opposing sense of vergence, seen in the two-dimensional cliff face in the lower series, is less common, and

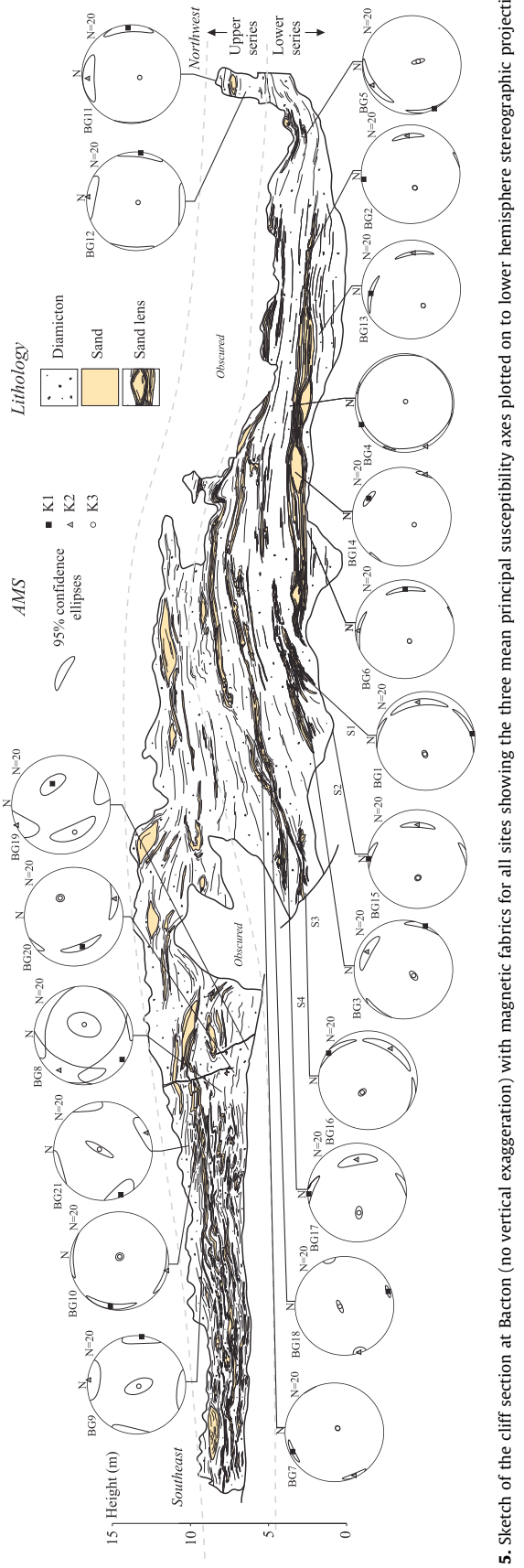

Fig. 5. Sketch of the cliff section at Bacton (no vertical exaggeration) with magnetic fabrics for all sites showing the three mean principal susceptibility axes plotted on to lower hemisphere stereographic projections.

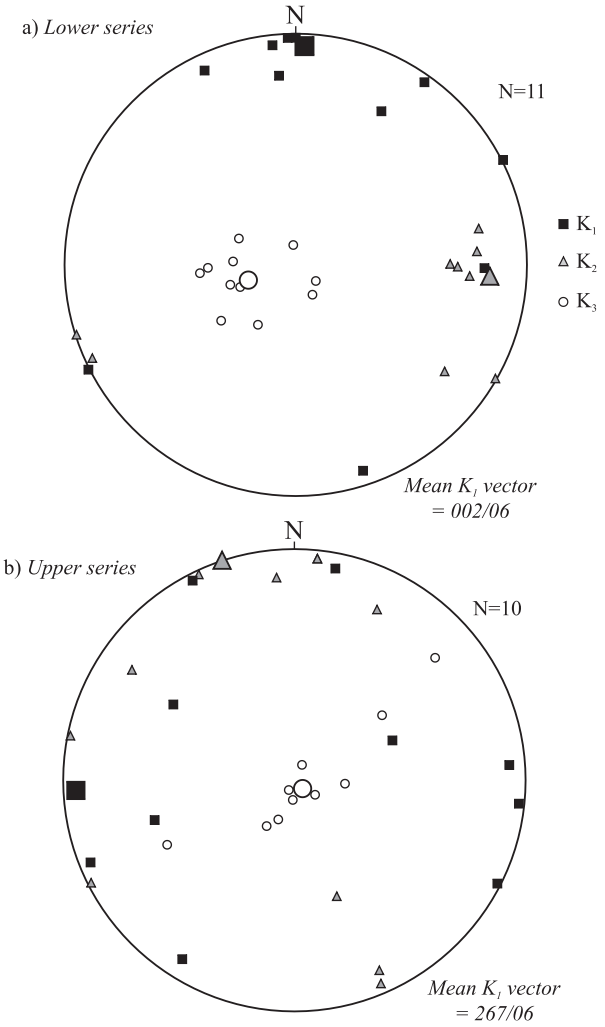

Fig. 6. Stereographic projections of the mean long (K_1), intermediate (K_2) and short (K_3) susceptibility axes of all sites sampled form (a) the upper series and (b) the lower series.

an apparent vergence to the southeast (on the two-dimensional cliff face) dominates. (Fig. 11a, b and d). Sheath folding is still prevalent with axes slightly to highly curvilinear, and there is evidence for superimposed folding (Fig. 11e). Stereographically, fold axes produce a girdle of orientations in a plane dipping to the west, with a weak clustering in the northeast quadrant (Fig. 9b). AMS fabrics within the upper series yield lineation data that generally clusters east-northeast–west-southwest (Fig. 6b). This fits on the girdle of fold axes and is generally parallel to the vergence directions observed.

5.3.2. Stretching lineations

Within the lower series, stretching lineations are observed on the surfaces of bedding (Fig. 10). In some cases these lineations form a striped pattern, where relief on the bedding surface stays roughly the same (e.g. Fig. 10a and b), whilst in other cases they mark steps in the position of the surface (e.g. Fig. 10c and d). Stretching lineations, measured from the lower series, form a tight cluster plunging 03–016° (Fig. 9c), at almost exactly the same orientation as the clustering of the axes of sheath folds (Fig. 9a) and the mean direction of the magnetic lineations (Fig. 6a).

5.3.3. Sand lenses

Lenticular bodies of sand exist within both the lower and upper series. Within the lower series, three main lenses are observed,

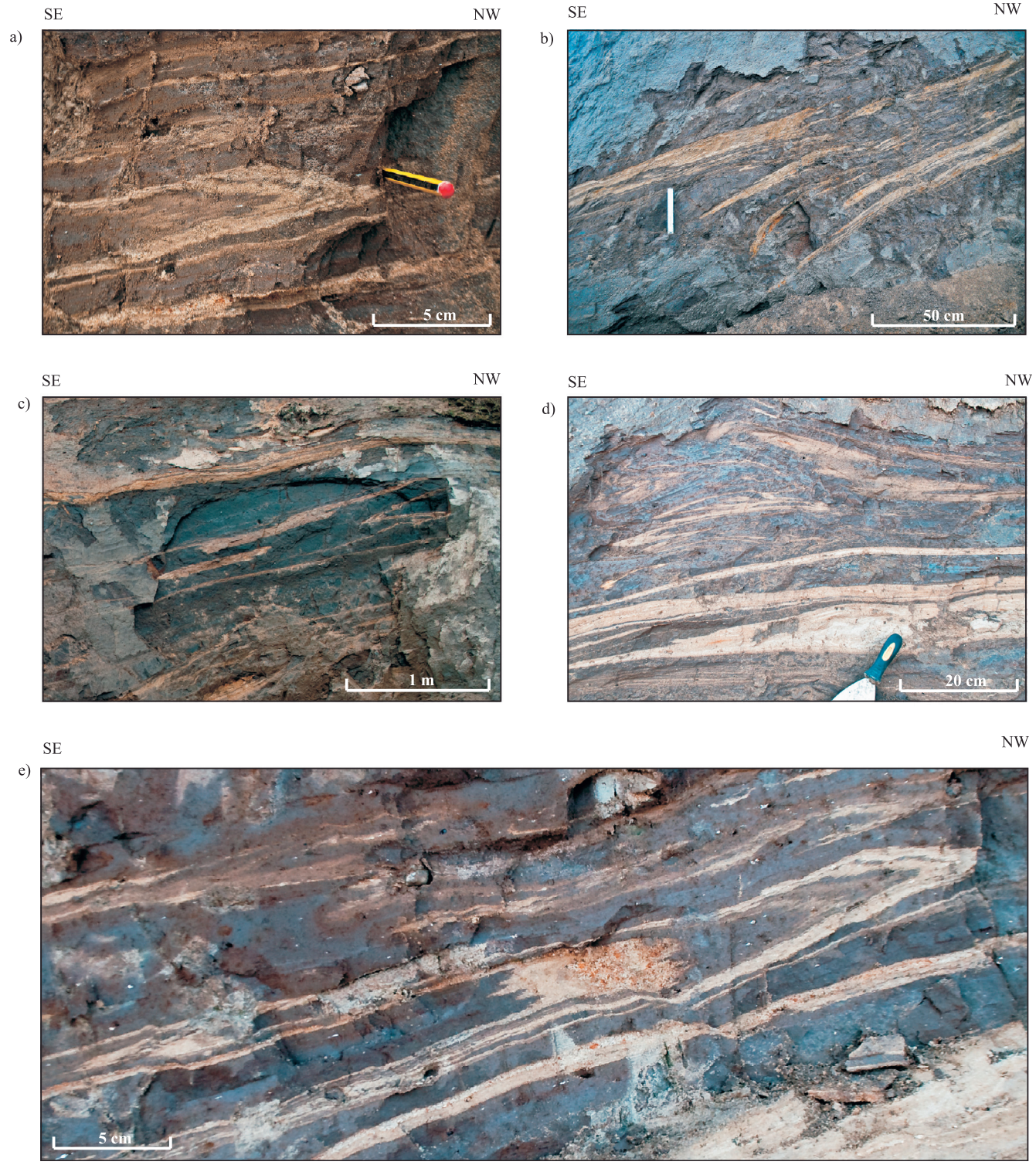

Fig. 7. Photographs of the typical structures associated with the ductile deformation of the lower series. (a) Isoclinal recumbent sheath fold showing parasitic folds around the hinge. Pencil marks the trend of the fold axis. (b) Series of highly curvilinear sheath folds with highly attenuated, boudinaged limbs forming sand "stringers". (c) Sheath folding resulting in a double vergence pattern and "eye" shaped lenses of sand. (d) Subhorizontal bedded sand passing into highly attenuated folds. (e) cm-scale parasitic fold on a m-scale sheath fold overprinted by Phase 3 steeply brittle faulting.

with a maximum height of 80 cm (Fig. 12). They are surrounded by sand layering (S1 in Fig. 2), which can clearly be seen to wrap around the lens, above and below. The contacts with the sand layering are parallel, and there is no evidence for erosion as would be expected if a subaqueous origin, through channel erosion and fill, were envisaged. Each of the three main lenses originates from separate sand horizons and is formed in progressively lower beds, to the northwest of the section (Fig. 12c). Interbedded diamicton can be seen to pinch out above and below the lenses, and thicken between lenses. Minor folding is evident in the zones on either side of some of the lenses (right of Fig. 12a). Partial excavation reveals that long axes are continuous into the exposure and are likely to be linear in form, with azimuths trending roughly northeast–southwest (Fig. 12c).

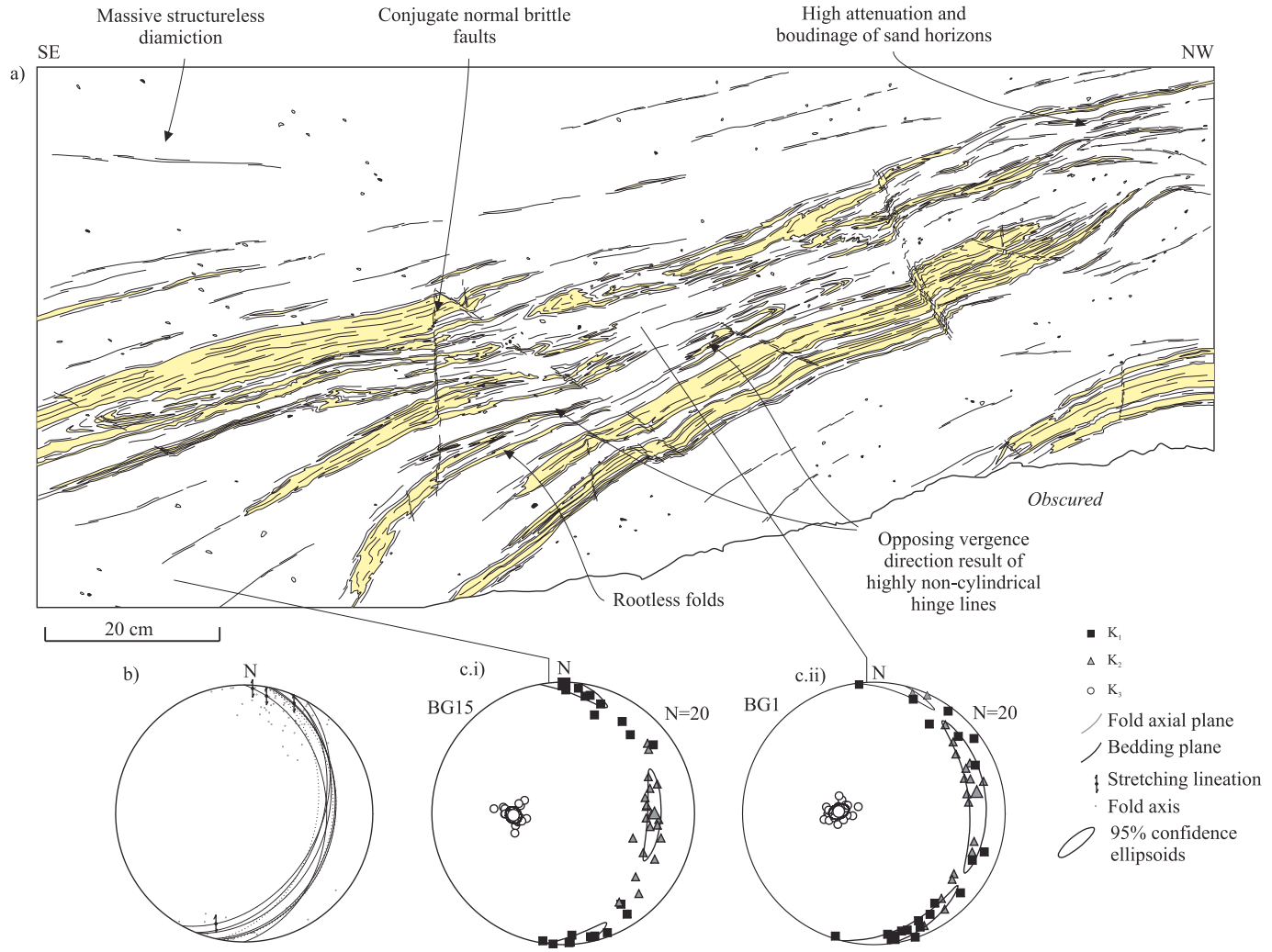

Fig. 8. (a) Field sketch of the styles of deformation within the lower series, with diamicton (white) and sand (yellow). Ductile structures include isoclinal, recumbent sheath folds with highly attenuated and boudinaged limbs. Also seen are the effects of Phase 3 brittle deformation showing conjugate normal faults under tensile stresses. (b) Stereographic projections of magnetic and structural data taken from location. (c) Stereographic projection of AMS fabric data from (i) BG15 and (ii) BG1. (For interpretation of the references to color in this figure legend, the reader is referred to the web version of the article.)

The sand lenses in the upper series show different characteristics (Fig. 13). They typically have a greater degree of asymmetry and do not show the underlying and overlying stratification that characterises sand lenses from the lower series. Sand horizons, at the same stratigraphic level as the lens, are not extensive and form tail-like patterns, which presumably were once connected to bedding and now appear to trail behind the lens (e.g. Fig. 13c), indicating movement top to the right and shear kinematics to the east.

AMS fabrics were analysed from the middle sand lens in the lower sequence (sample BG14, Fig. 12d), which had a more clay-rich matrix than the others, facilitating sampling and suitability for magnetic analysis. A strong clustering of the K_1 axes is observed plunging 25–029°, parallel to nearby stretching lineations on bedding surfaces and subparallel or slightly inclined to the axial trend of the lenses.

5.3.4. "Brittle" structures

The term fault is used to describe sediment that has failed in a brittle-like manner with deformation isolated along discrete centimetre-scale shear zones separating blocks of undeformed sediment (or with at least unrelated deformation). Faults are located throughout the section and typically are both extensional (Fig. 14a, b and d) and occasionally reverse (Fig. 14c). They can clearly be seen to cut the gently dipping isoclinal folding and limb attenuations and as a result, must post-date the original structures.

Most of the faults are moderately to steeply dipping (>70°) and in places form in two dominant orientations, with opposite sense of displacement constituting a conjugate pair (Fig. 14d and e). Displacement is low, up to 10 cm in the upper series, but typically less than 2 cm in the lower series. Other than the conjugate pairing, the faults show a range of orientations and produce no consistent pattern in terms of shear in any particular direction (Fig. 14f). The faults are distributed within the sand lamination and probably continue into the diamicton, but a lack of markers make displacements difficult to discern. Deformation along fault planes takes place in zones ranging from <0.5 mm to >5 cm (Fig. 14b), probably by the means of grain rolling, boundary sliding and the breaking of weak bonding cements that may have formed; a process commonly referred to as granular flow (Twiss and Moores, 1992). This process is probably analogous to the faults produced in sand box models (McClay and Ellis, 1987). In some larger fault zones, displacement occurs along a network of smaller shears rather than distributed evenly across the zone.

As deformation is confined to the faulted zones, the bounding blocks have not been pervasively deformed during this event, which suggests that the AMS fabric has been largely unaffected; however, the deformation associated with the formation of the

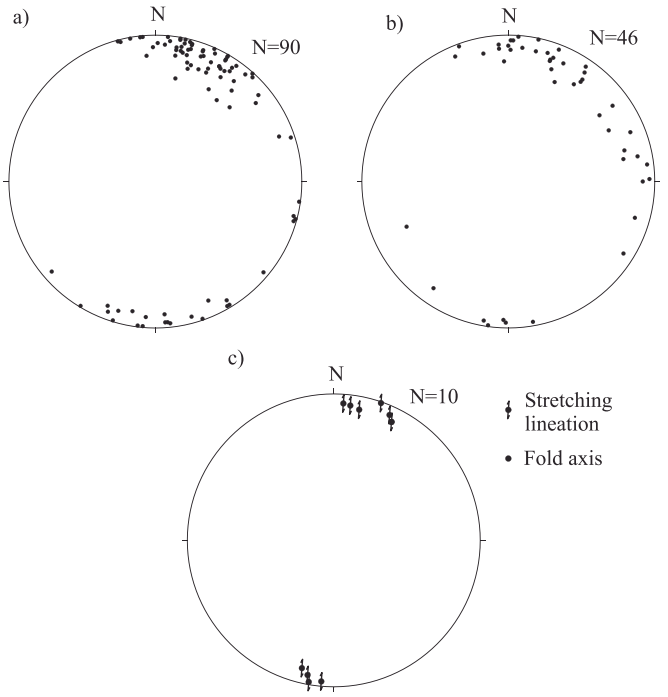

Fig. 9. Stereographic projection of Phases 1 and 2 structural data collected from the lower and upper series. (a) Fold axes from the lower series. (b) Fold axes from the upper series. (c) Stretching lineations from the lower series.

bands has gently tilted the strata. As such, the orientations of axial planes of folds and foliations have also been somewhat reorientated. Therefore, their imbrications cannot be used as kinematic indicators for direction of shear. Similarly imbrications of the magnetic lineations cannot be used solely to determine kinematics as has been done in previous AMS studies of sheared till (Iverson et al., 2008; Shumway and Iverson, 2009; Thomason and Iverson, 2009).

5.3.5. Sand-filled fractures

Sand-filled structures were observed in the upper series at one location (Fig. 15). The largest is 4 m in height and up to 30 mm in width, extending to the top of the exposure. The sand is fine to medium and is of a similar composition to sand elsewhere within the sequence. The fractures are typically planar in form and dip steeply to the west–southwest at the same orientation as nearby faults. They are usually irregular in form and deviate slightly across bed boundaries where they sometimes splay into surrounding diamicton, e.g. the sand "intrusion" in Fig. 15. The thickness of sand within the fractures varies to up to 30 mm and there is a general increase in thickness towards the top.

The sand-filled fractures are at the same orientation as faults within the immediate vicinity and are steeply inclined (>70°), with a reverse offset which displaces stratification on either side of the fracture by up to 10 cm. As they overprint previous structures, they must post-date the phases of ductile deformation, and their orientation suggests formation during or after faulting. As with the faults, their orientation bears no relationship to the local stress

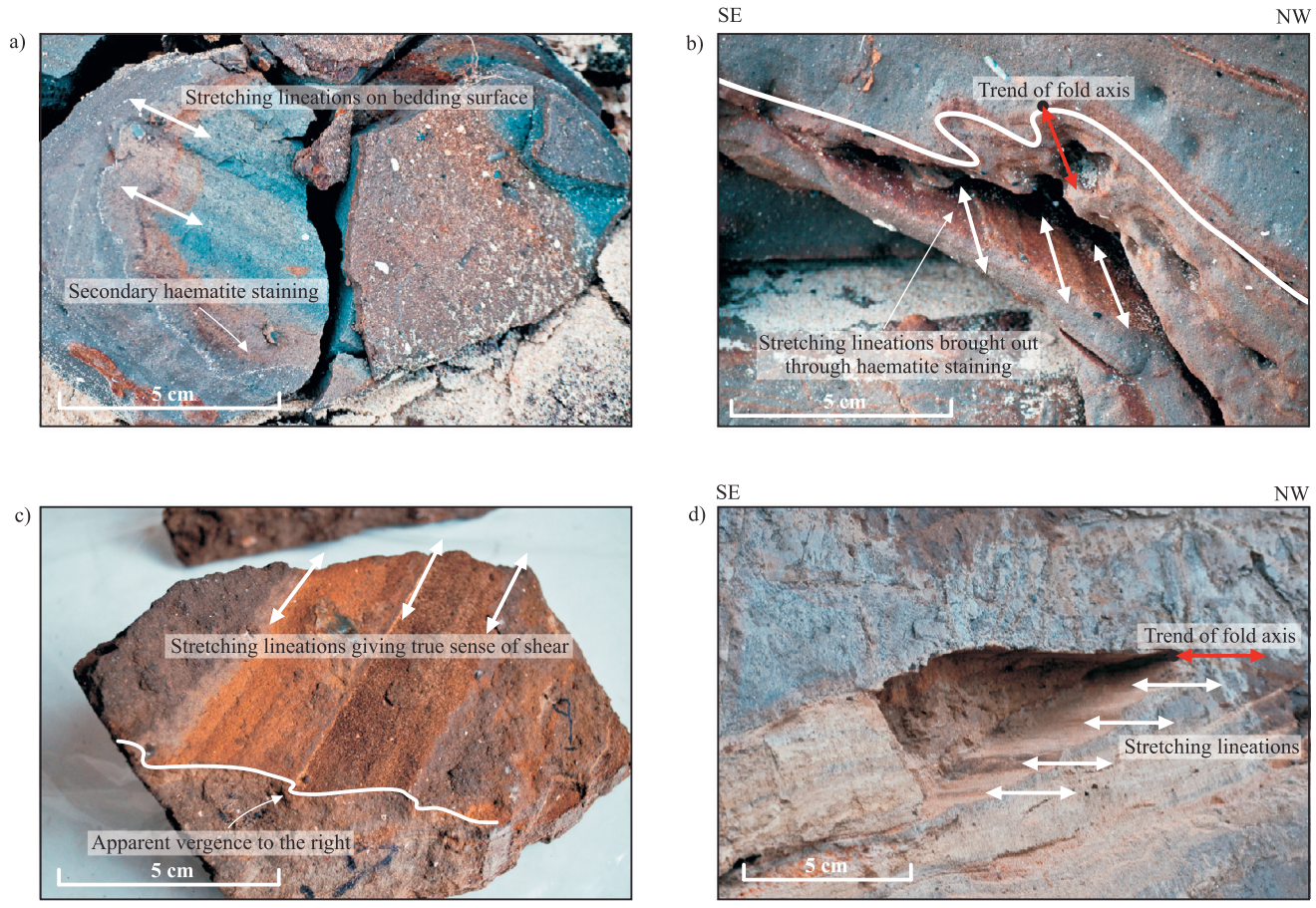

Fig. 10. Photographs of stretching lineations associated with Phase 1 ductile deformation of the lower series. (a) Stretching lineation on the bedding surface of a sand layer within the diamicton. (b) Stretching lineation at the axis of a sheath fold orientated parallel to the axis of the fold, suggesting shear into the exposure in spite of apparent vergence to the left. (c) Impregnated block of diamicton showing stretching lineation on the bedding surface giving an apparent vergence direction to the right. Brown colouration denotes haematite staining. (d) Stretching lineation showing pronounced stepped nature orientated parallel to the axis of the sheath fold. (For interpretation of the references to color in this figure legend, the reader is referred to the web version of the article.)

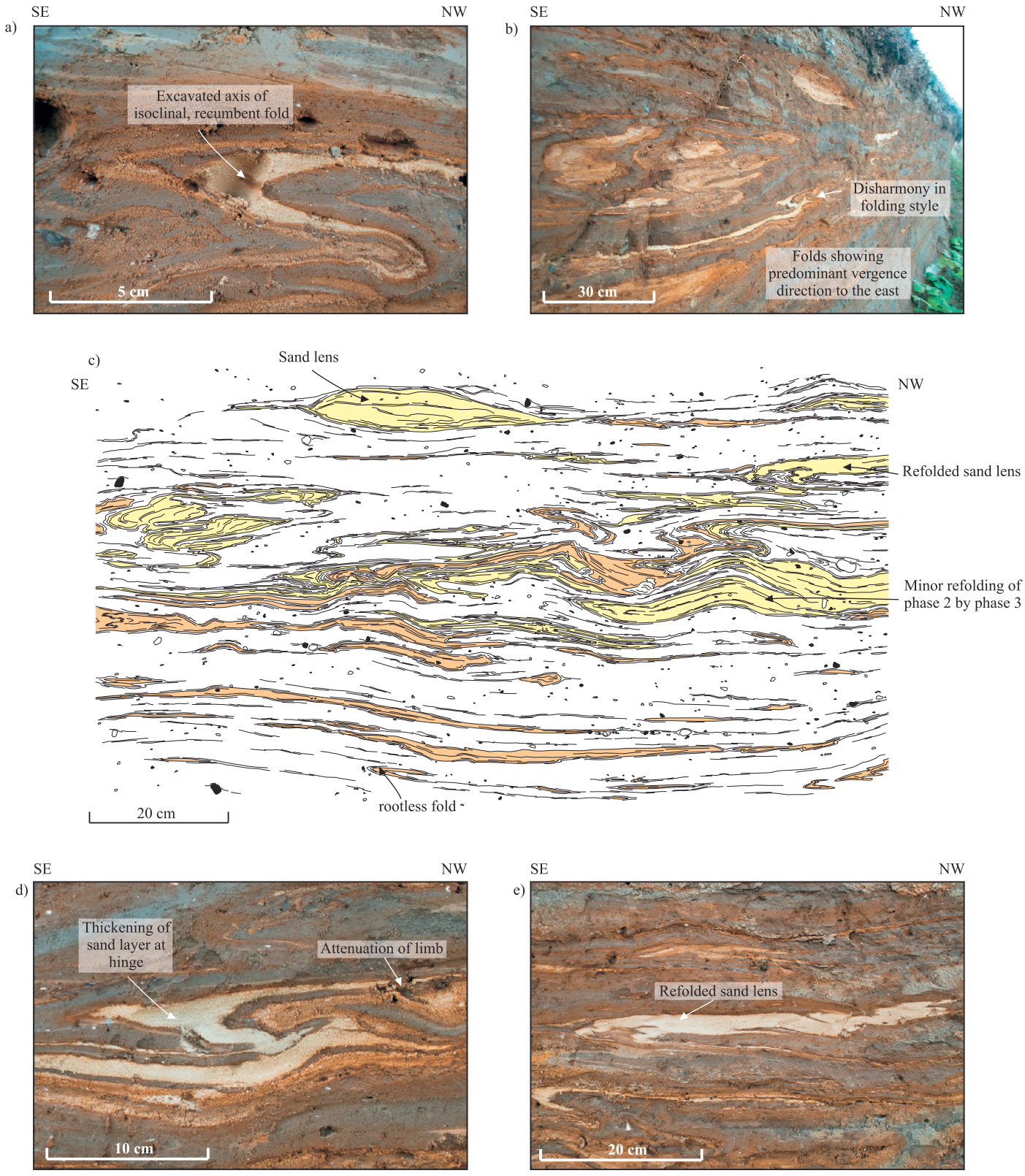

Fig. 11. Photographs and sketch of Phase 2 structures within the upper series. (a) Excavated fold axis of an isoclinal, recumbent fold illustrating how the unconsolidated nature of the sediment facilitates the collection of structural measurements. (b) Cliff section showing disharmonic folds with a dominant vergence direction to the left. (c) Sketch of a typical section of the upper series showing the styles of folding with diamicton (unshaded) and sand (shaded). d) Isoclinal, recumbent fold within a sand layer showing pronounced thickening around the hinge and attenuation and thinning of the limbs. (e) Refolding of a sand lens, suggesting a progression of the strain field from extension to compression as a result of the overprinting of deformation events.

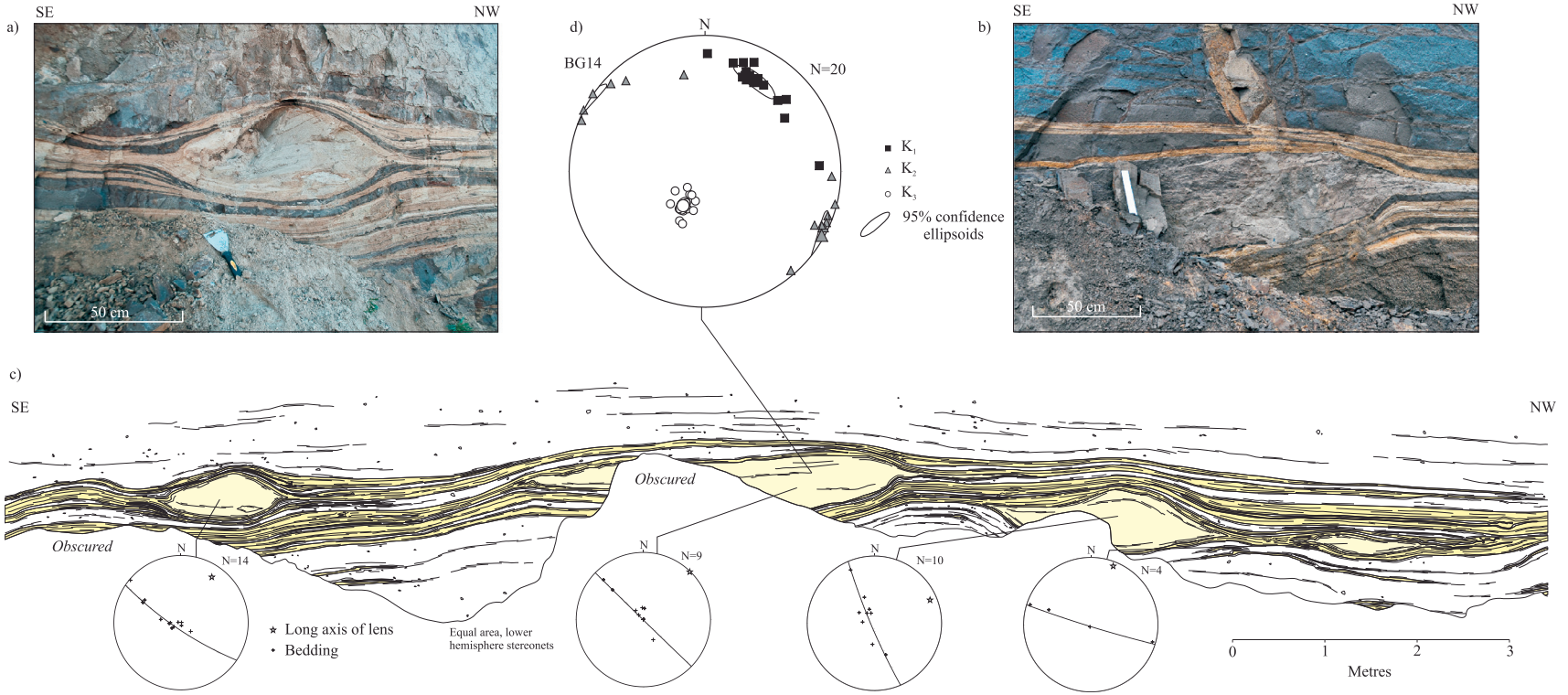

Fig. 12. Photographs and sketches of sand lenses from the lower series with structural and AMS data. (a) Photograph of sand lens from the lower series with asymmetry and parasitic folding suggesting shear influenced formation to the south. (b) Photograph of sand lens with clay matrix where AMS sample BG14 was collected. (c) Sketch of sand lenses across the lower series. Each lens originates from its own sand horizon at progressively lower intervals to the right of the photo. Attached are stereographic projections with poles to the contacts (black crosses) around the outside of lens with great circle fitted to indicate the axial trend of the lens (stars). (d) Stereographic projection of sample BG14 showing the (K_1), intermediate (K_2) and short (K_3) axes of the susceptibility ellipsoid from all subsamples.

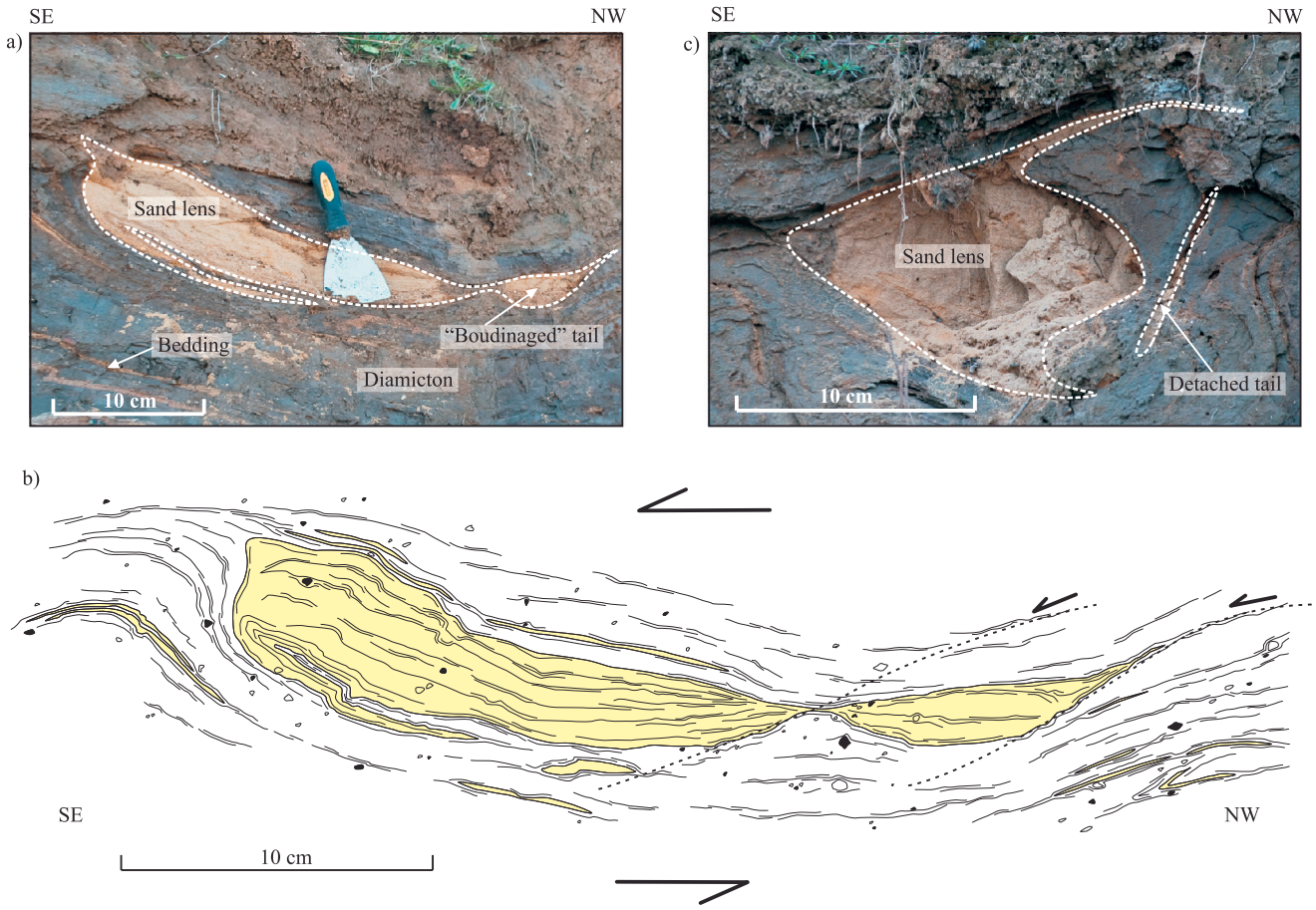

Fig. 13. Photographs and sketch of sand lenses from the upper series. (a) Asymmetric sand lens with tails trailing behind lens to the west with a portion becoming boudinaged. (b) Sketch of the same sand lens showing relationship to stratification. (c) Asymmetric sand lens with tails disconnected from the surrounding horizons.

conditions inferred by previous structures, and as deformation is restricted to the a discrete zone, these are not likely to have any major effect on the AMS fabrics other than minor tilting.

6. Interpretations

6.1. Magnetic mineralogy

Investigations into the magnetic mineralogy reveal that a range of magnetic mineral phases is present. AF-demagnetisation and IRM acquisition reveal that high and low coercivity phases, presumably low-Ti titanomagnetite and haematite exist; however, susceptibility and thermomagnetic experiments indicate that these are not in sufficient quantities to dominate the AMS signal. Thermomagnetic analyses and low temperature susceptibility experiments indicate that a paramagnetic phase controls the AMS. The identification of low-Ti titanomagnetite and haematite, whilst they are not controlling susceptibility, do suggest a strong potential for further palaeomagnetic investigations utilising secular variations in the Earth's magnetic field as a relative dating tool (cf. Butler, 1992). Petrological examination reveals that the coarser components are largely diamagnetic quartz and shell fragments which have a negligible susceptibility when other paramagnetic and ferromagnetic phases are present, so it is assumed that the paramagnetic carrier lies within the clay matrix. Previous XRD analysis has revealed that the clay mineralogy of the Norfolk tills is dominated by chlorite, illite and kaolinite and therefore the magnetic susceptibility is likely to be dominated by these phyllosilicate minerals; however, fabrics may be locally affected or enhanced by the ferromagnetic phases discussed above.

Although Iverson et al.'s (2008) AMS fabrics were controlled by magnetite grains, here a paramagnetic phase has been identified, probably chlorite, which is controlling the AMS. During shear, the basal planes of clay minerals will rotate into the most stable orientation. This is parallel to the plane of shearing and therefore will tend to be more sensitive to compressive strain and produce an oblate fabric. Magnetic lineations can be produced by platy clay minerals (Cifelli et al., 2005, 2009; Mattei et al., 1997; Parés and van der Pluijm, 2002), where basal planes are disposed about a common axis parallel to stretching (Cifelli et al., 2005). Comparisons with neutron diffraction measurements have shown that AMS of sediments, where a clay fraction is carrying the susceptibility, can successfully be used to quantitatively describe mineral fabrics (Cifelli et al., 2009). At the study site, the correlation between the trend of structures (fold axes and stretching lineations) with the magnetic lineations (e.g. Fig. 8b and c) show that this interpretation is also valid. Therefore, the orientations of magnetic lineations, verified through structural measurements, are considered an accurate representative of the stretching direction during progressive simple shear.

6.2. Deformational style and genesis

The mechanisms of deformation of the North Norfolk Quaternary glacial sequences have been debated. Most authors agree that glaciotectonic deformation is responsible for most of the structures

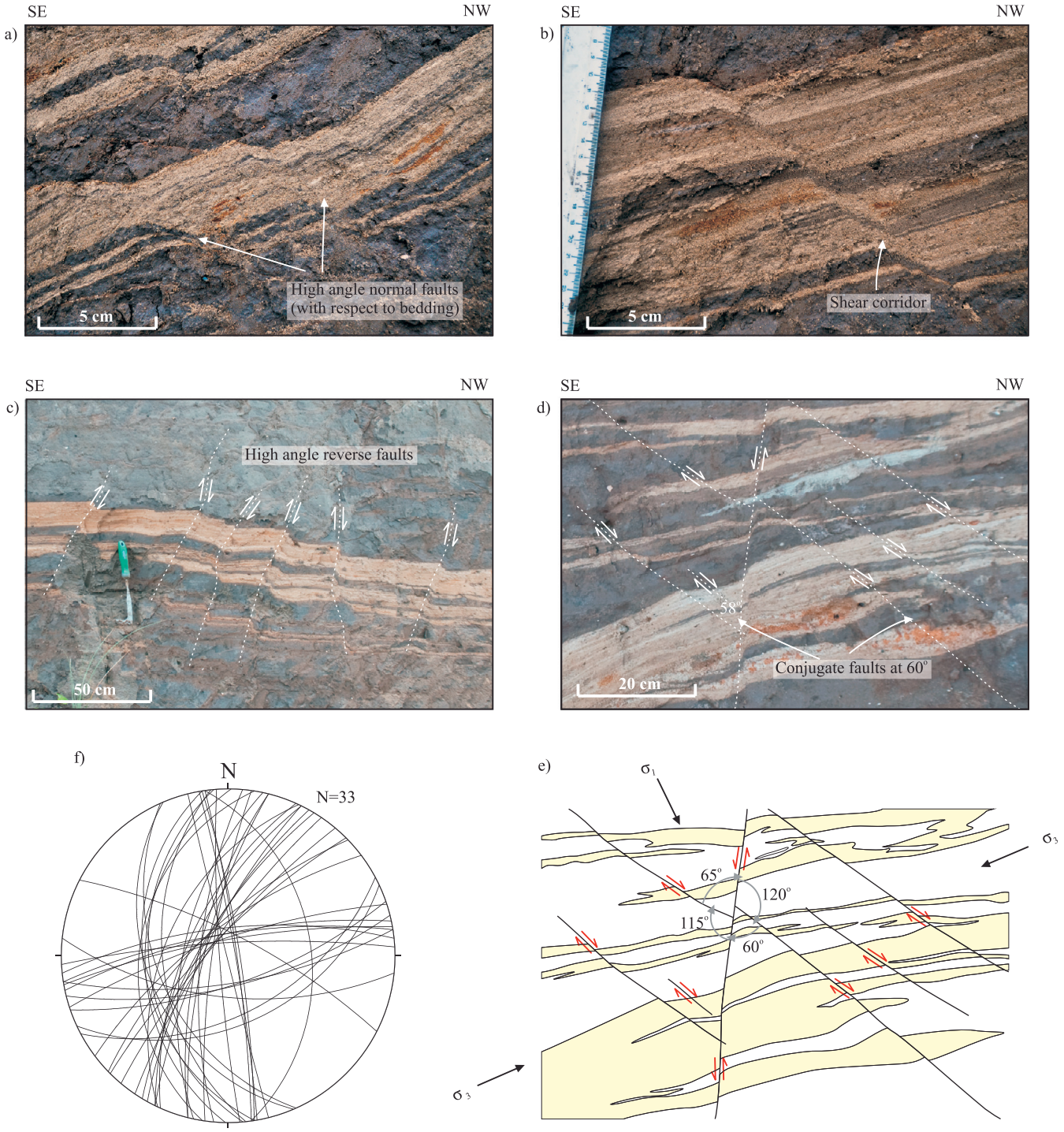

Fig. 14. Brittle structures associated with Phase 3 deformation. (a) Low-angle faults dipping to the north showing a normal displacement. (b) Close up of fault showing that movement is accommodated through a 10 mm wide shear zone, presumably through processes of granular flow. (c) Steeply dipping reverse faults showing apparent reverse offset. (d) Photograph and (e) sketch of conjugate faults forming at predictable orientations, revealing formation dominated by subhorizontal tensional stresses. (f) Stereographic projection of planes of faults within both the upper and lower series.

seen within the Bacton Green Till Member (Banham, 1965, 1988; Banham and Ranson, 1965; Phillips et al., 2008; Roberts and Hart, 2005), although Eyles et al. (1989) have argued for a subaqueous origin through subaqueous sliding and mass movement. There are similarities between both styles of deformation, but the process driving the deformation is distinct in each case. In a subglacial environment, deformation is controlled by the movement of the glacier, and although perturbations in flow exist, the dominant process of deformation is because of simple shear and the strain pattern should reflect this (Hart and Roberts, 1994). Within areas affected by slumping and sliding, deformation would be expected to be restricted to local failure planes, and sediments away from these planes are largely undeformed (Hiemstra et al., 2004). At Bacton, except for a switch in orientation within the upper series, magnetic fabrics are generally consistent (Fig. 5), indicating that deformation is largely pervasive throughout the section. This, combined with the abundant structures typical of subglacial shear (boudins, sheath folds and stretching lineations) leads to the

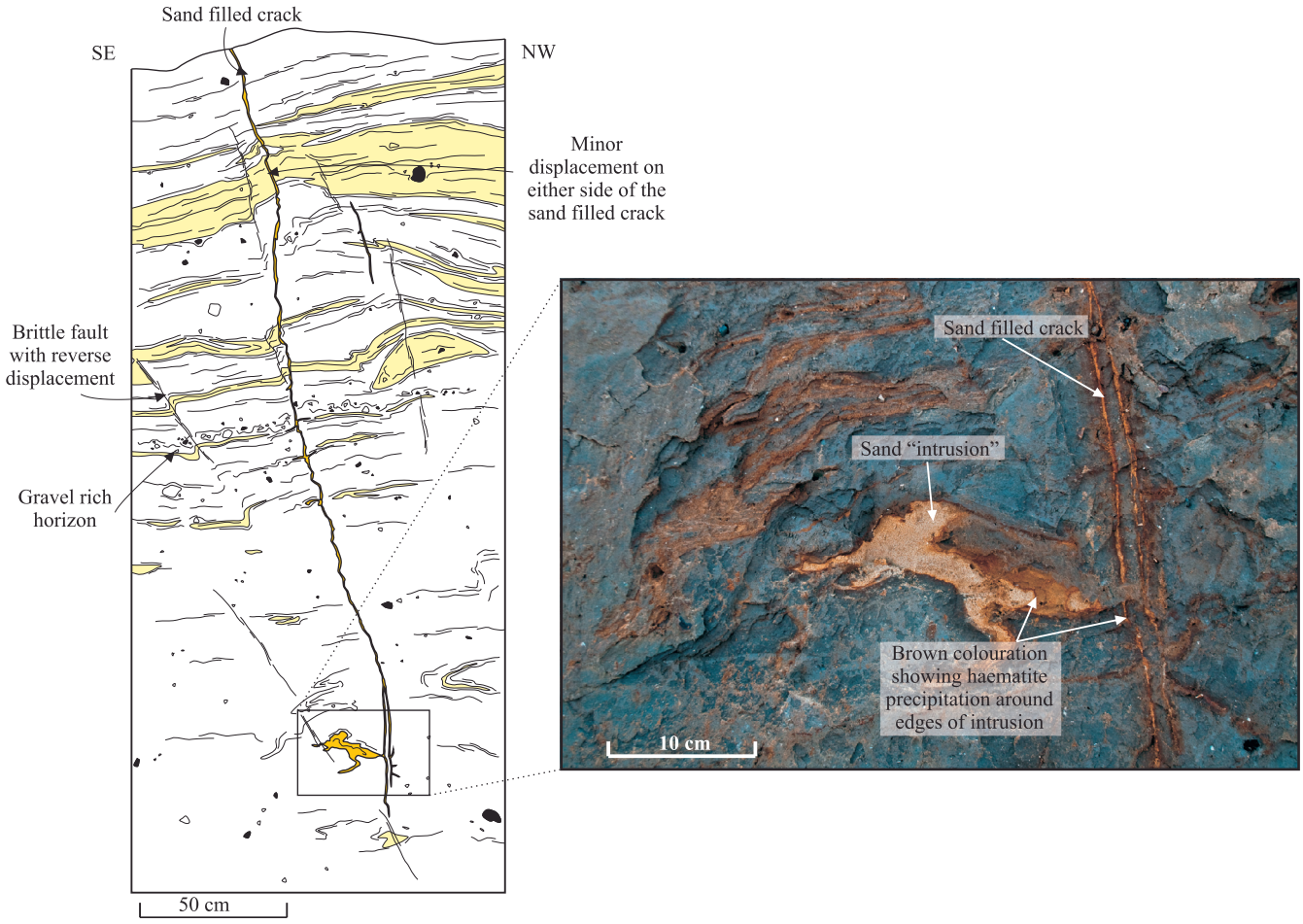

Fig. 15. (a) Sketch of a sand-filled crack and sand intrusion within the upper series of the Bacton Green Till Member with sand within the sand filled crack (yellow), stratification sand (pale yellow) and diamicton (white). (b) Photograph of sand filled crack and sand intrusion into diamicton. (For interpretation of the references to color in this figure legend, the reader is referred to the web version of the article.)

interpretation that glaciotectonism is the dominant mechanism for ductile deformation at this location.

Glaciotectonism has resulted in a folding style, typical of progressive simple shear. Compressional deformation dominates the initial stages of shear and folding occurs where there are layers with sufficient interlayer contrast in strength. As the shearing progresses, constriction becomes dominant and the strain ellipse migrates to a lower angle to bedding, resulting in attenuation of fold limbs and boudinage. Folds subsequently become highly asymmetrical and attenuated, with axial planes almost parallel to the bedding to the direction of shearing. Under these circumstances, fold axes tend to rotate to an orientation parallel to the direction of shearing creating a highly curvilinear style folding referred to as sheath folding (Alsop and Holdsworth, 2004; Alsop et al., 2007).

Sheath folding is a phenomenon that is commonly recognised within glaciotectonised sediments (e.g., Kluiving et al., 1991; Lesemann et al., 2010; Smith, 2000; van der Wateren, 1999) and within glacier ice itself (e.g., Goodsell et al., 2002; Hambrey and Huddart, 1995). The recognition of sheath folding in the Bacton Green Till Member is key to understanding glacial transport directions, as in a two-dimensional section, sheath folding can produce contradictory vergence directions. Only through detailed structural measurements can shear direction be calculated. This could possibly explain discrepancies between the direction of stretching lineations, pebble fabrics and observed vergence directions at other sections, e.g. the presence of stretching lineations orientated subparallel to fold axes in Phillips et al. (2008) and contrasting fold directions and pebble fabric orientations in Hart (2007).

6.2.1. Stretching lineations

Stretching lineations form either due to the smearing out of subtle variations in mineralogy on the bedding surface, or where they form a stepped nature, as a result of the realignment of linear features e.g. axes of parasitic folds parallel to the direction of stretching. Similar lineations have been noted by (Phillips et al., 2008) within the Bacton Green Till Member at a section between West Runton and Sheringham; however, these were attributed to a phase of deformation unrelated to folding. Within the section at Bacton, the stretching lineations lie parallel to the orientations of sheath folds and magnetic lineations (e.g. Fig. 7b and c). It seems probable, therefore, that they are linked and support a local strain field within the lower series dominated by north–south stretching.

6.2.2. Sand lenses

Lenses of sand and chalk have been described in numerous localities along the Norfolk coast (e.g. Hart, 2007; Hart and Boulton, 1991; Lee and Phillips, 2008; Phillips et al., 2008; Waller et al., 2011) and several interpretations proposed for their origin (cf. Waller et al., 2011). Phillips et al. (2008) suggested, based on heavy mineral compositions, that the sands were derived from the underlying Mundesley Sand Member by thrusting and fragmentation during a brittle phase of subglacial deformation. However,

continuous sand layers and diamicton wrap and flow around the lenses (Fig. 12a–c), consistent with boudinage and inconsistent with thrusting. Magnetic lineations from sample BG14, taken from inside a sand lens (Fig. 12d), reveal stretching in a north-northeast–south-southwest orientation, consistent with magnetic lineations and structural measurements taken nearby, indicating they formed during the same north–south stretching event.

6.2.3. Brittle faults

The faults record a brittle phase of deformation that must have occurred after the initial phase of ductile deformation as pre-existing structures are overprinted. At the study site, Lee and Phillips (2008) recorded low-angle to moderately inclined thrusts and moderately dipping normal faults, which may be Riedel shears (Riedel, 1929) associated with a glaciotectonic shearing event to the north. The orientations of structures, however, provide a challenge to this hypothesis. The majority of the faults have a normal offset, forming conjugate pairs. They are predominately moderate to steeply dipping and show no relationship to strains predicted either by magnetic fabrics, or from shear in a specific direction. Low-angle thrusts (P shears) and normal faults (R_2 shears), that typically form in association with Riedel shears, were not observed. Instead, all brittle structures were steeply dipping. It is proposed that the simplest explanation for these faults is that they occurred during dewatering and lateral extension associated with loading and compaction during rapid deposition of sands and gravels of the overlying Briton's Lane Formation. Under these circumstances, faults with a reverse offset can form, either by the progressive rotation of normal offset faults, or through minor flow and remobilisation during loading.

6.3. Revised model of the deformation of the Bacton section

The results presented support previous interpretations that indicate the primary mode of deposition was associated with an advancing ice sheet into a glaciolacustrine basin (Lee and Phillips, 2008; Phillips et al., 2008), whereby diamicton was deposited by underflows and rainout, and sand laid down as turbidites, all of which was subsequently overridden by ice and glaciotectonically deformed. The combined analyses of magnetic fabrics and visible structures has revealed that the sequence has been affected by at least two contrasting directions of simple shear and extension, therefore, the deformation model of Lee and Phillips (2008) can be modified as follows:

Phase 1 – Subglacial glaciotectonism and north–south stretching associated with progressive simple shear. Pervasive ductile deformation occurring as a result, producing magnetic lineations through the disposition of clay mineral basal planes about a common axis, sheath folds, the attenuation of fold limbs and the boudinage of sand horizons.
Phase 2 – Subglacial glaciotectonism and east–west orientated stretching restricted to the upper series only. A switch in direction of pervasive ductile deformation occurring as a result, causing the realignment of clay minerals and therefore magnetic lineations, and the refolding of folds and boudins. The reduction in thickness of deformation may be related to a change in the hydrological properties of the sediment or allochthonous thickening of the sedimentary pile.
Phase 3 – Compaction, dewatering and loading of the Briton's Lane Formation, shortly after glacial retreat. Variations in lithology cause inconsistencies in the amount of compaction laterally, and stress is accommodated along brittle faults in a less dilated state, to accommodate strain. Water and fluidized sand is expelled from the sequence through fractures forming the sand filled cracks.

7. Discussion

7.1. Regional ice flow

Magnetic fabrics, stretching lineations and the trend of sheath folds reveal initial stretching north–south but switching to east–west, as a result of glaciotectonically induced simple shear. Asymmetrical folds and boudins, within the upper series, indicate that this east–west orientated stretching is the result of east-directed shear. If it is assumed that this shear is parallel to glacier flow (which may not necessarily be the case as in Piotrowski et al. (2004), then this would indicate east-directed ice flow (Fig. 16c). This would support previous work on the Bacton Green Till Member and corresponds well to the regional ice flow that deposited the Weybourne Town and Lowestoft Till Members (e.g., Fish and Whiteman, 2001; Phillips et al., 2008; Scheib et al., 2011; West and Donner, 1956)

More problematic is relating the initial north–south stretching to a particular ice flow direction due to the ambiguities of sheath folding and the presence of bedding-parallel structures, typical of Phase 1 deformation. Furthermore, during the occurrence of Phase 3, previous structures have been reorientated. As such, the subtle imbrications of planes and lineations cannot reliably be used as kinematic indicators as has been done previously. Lee and Phillips (2008) and Phillips et al. (2008) suggested that the retreat of the margin of an ice body to the north, allowed ice from the southwest to advance into a temporary basin that was created between the two ice sheets (option 1 in Fig. 16b). Under this model, northerly-directed shear associated with local flow from the southeast could be envisaged (option 2 in Fig. 16b). However, northerly-directed flow seems unlikely given the clast provenance of the glacial deposits of North Norfolk. For example, the Weybourne Town Till, which may have been deposited by the ice that deformed the Bacton Green Till Member elsewhere (Phillips et al., 2008), has a provenance from the North Sea (Hamblin et al., 2005). Other authors suggest that the member was deformed by ice from the north, possibly associated with the same south flowing ice advance that deposited the member (option 2 in Fig. 16b). As such, two possible ice flow vectors are proposed during Phase 1, which, assuming ice flow is parallel to stretching, could be used to explain the Phase 1 pattern of deformation seen at the locality.

Recent numerical modelling (Boulton and Hagdorn, 2006; Hubbard et al., 2009) of the British and Irish ice sheet during the last glacial period has suggested highly dynamic glaciation, with ice being drained largely by a number of transient, switching ice streams, and it is likely that similar concepts could be applied to earlier, Middle Pleistocene ice sheets. Dynamic glaciation within a single ice sheet could be enough to explain the flow vectors and polyphase deformation reported. Moreover, the likely presence of interacting lobes of British ice and Pennine ice provide possible scenarios under which the reported flow vectors and polyphase deformation could occur.

7.2. The use of AMS for glaciotectonic studies

This study has shown that AMS fabrics reflect the preferred alignment of minerals within a glaciotectonite. It therefore directly reflects strain acting on the site through glaciotectonic processes. Magnetic lineations are parallel to stretching lineations and the clustering of fold axes, which suggest that they reflect stretching during progressive simple shear as a result of subglacial glaciotectonism. Therefore, the structural data corroborates the AMS results and supports the interpretation that AMS can be used to accurately evaluate strain within glaciotectonites.

The key advantage of AMS, over other petrofabric techniques, is that strain can accurately and rapidly be determined in three

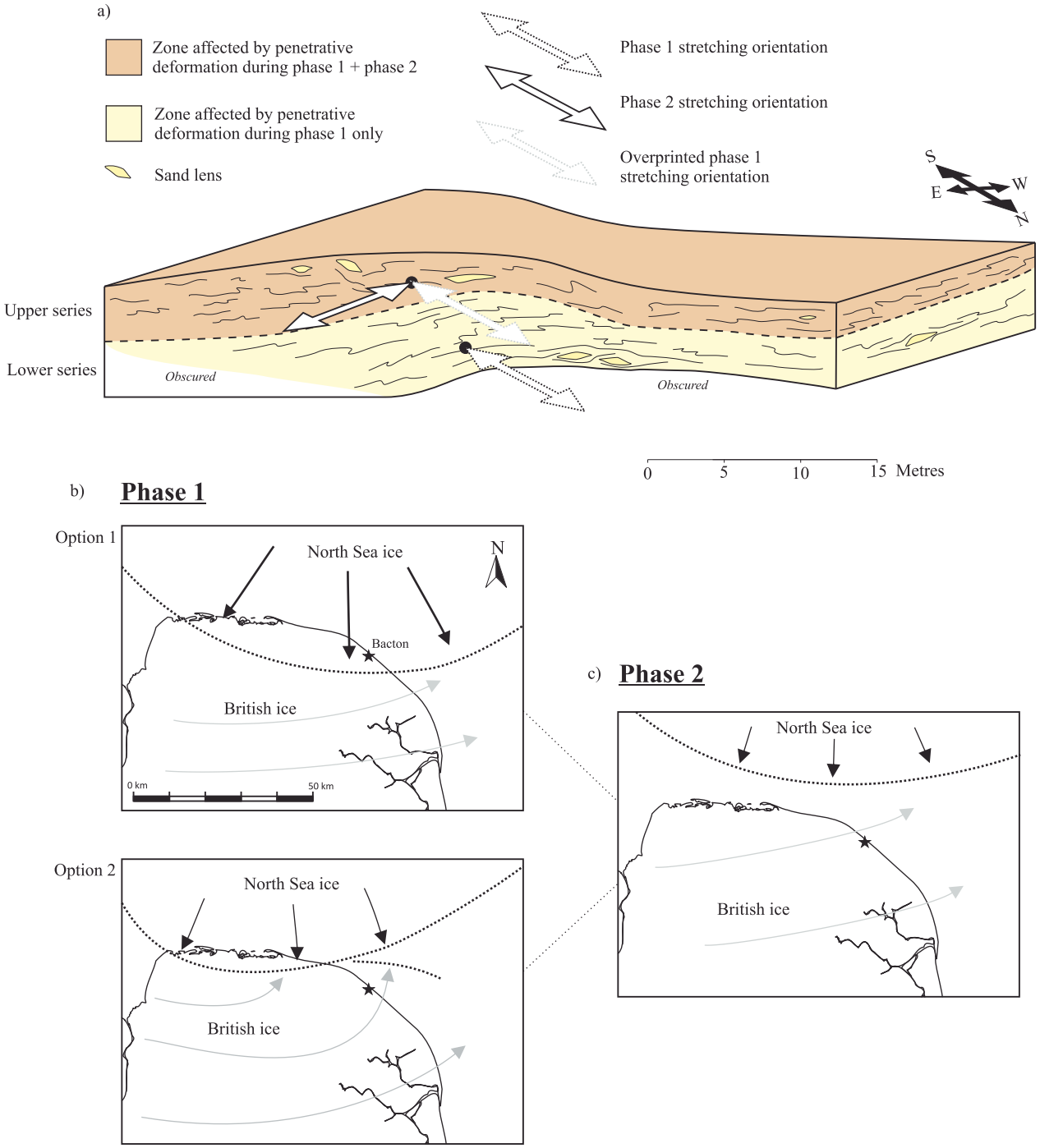

Fig. 16. Revised model for glaciotectonic deformation of the Bacton sequence. (a) Stretching directions during shear strain during Phase 1 and Phase 2 deformation. Possible scenarios for ice flow patterns based on previous suggestions (Fish and Whiteman, 2001; Phillips et al., 2008; Scheib et al., 2011; West and Donner, 1956) during (a) Phase 1 and (c) Phase 2 deformation. Scenarios are based on the assumption that ice flow is parallel with direction of simple shear within the sediment, which may not necessarily be the case.

dimensions. Utilising the methodology described, blocks can be impregnated and cut in a few days, and each subsample measured in the Kappabridge in minutes. As the process is automated, the only potential for error is from the initial measurement of the orientation of the sample. The spatial resolution of the AMS technique is also far better than pebble fabric and structural measurements. Moreover, fabrics from each subsample reflect the volume averaged of many grains within a sample, and an average of 18 subsamples is used to calculate mean fabrics from a site. The technique does not rely on a lithology where structures can be seen, and can thus be used on the many structureless tills. AMS, however, needs to be applied with caution. It is an oversimplification to state that AMS reflects a preferred alignment of the long axis of mineral grains. In reality, tills can have a highly variable magnetic mineralogy and because of the different properties of different magnetic minerals (e.g. distribution, shape and crystallographic anisotropies) investigating the magnetic mineralogy is a critical step when interpreting magnetic fabrics. For example, if a similar mineralogy to that of Hooyer et al. (2008) was assumed, fabric strengths may be interpreted as being too weak to fit in with the bed deformation model and thus an alternative mode of genesis may have been envisaged. The magnetic mineralogy must therefore be investigated fully before interpretations can be drawn.

This study adds to the work of AMS for glacial sediments and builds on the work of previous authors by showing that AMS can show significant insights into patterns of glaciotectonic deformation, where paramagnetic clays dominate the magnetic susceptibility. This study opens up new possibilities for the investigations of glaciotectonism, and as the technique can be directly repeated and applied to other sections, has potential to add additional constraints on deformation styles and ice flow directions within the Quaternary of North Norfolk and elsewhere.

8. Conclusions

The sediment genesis and flow vectors of the Bacton Green section have been reinvestigated using a combined structural and magnetic approach. A number of conclusions can subsequently be drawn that throw light both on the glacial history of North Norfolk and the application of AMS to study glacially deformed sediment.

- Imprinted in the structures and magnetic fabrics of the Bacton Green Till Member are evidence of at least two phases of ductile deformation formed as a result of oscillations of North Sea- and British-based ice during the glaciations of the Anglian stage. Initially, north–south orientated stretching affected both the upper and the lower series, but was replaced by east–west orientated stretching affecting only the upper series.
- Magnetic fabrics are controlled by the preferred alignment of dominantly iron-bearing paramagnetic clay minerals. Magnetic lineations are formed by the alignment of the basal planes of these clay minerals about a common axis. These lineations are parallel to macroscopic structures (stretching lineations and sheath folds) and are an accurate representative of the stretching direction during progressive simple shear.
- The large amount of stretching within all layers, with no discrete guide planes and a lack of a known significant palaeoslope indicates that glaciotectonic deformation is responsible for ductile deformation during Phases 1 and 2. In contrast, Phase 3 brittle structures are dominated by conjugate faults, unrelated to shear in any particular direction, interpreted to have formed after glaciotectonism during loading, sediment compaction and dewatering.
- AMS, corroborated through structural measurements, has revealed subtle variations in strain direction presumably relating to ice flow and has given new insights in the deformation characteristics not previously possible within a glaciotectonised deposit. In particular, the importance of the realignment of linear features parallel to flow and as a result, the interpretation of stretching lineations and the clustering of fold axes has been illustrated.
- This study has built on the previous work of the examination of AMS of glacial sediments and shows that the strain field can be accurately measured within a glaciotectonite, where a paramagnetic fraction is controlling the susceptibility. This approach can be directly applied to other glaciotectonised localities and has the potential to provide significant insights into the sometimes complex history of glaciated areas.

Acknowledgements

This work forms part of the NERC funded GAINS (Glacial Activity in Neoproterozoic Svalbard) grant (NE/H004963/1) with a tied PhD studentship held by EJF. We would like to thank Tara Grove and Alan Fleming for their assistance in the field, the Ministry of Defence Police at Bacton for facilitating access to the site, the GAINS collaborators Doug Benn and Michael Hambrey for useful discussions, and Paul Hands for the production of thin sections. We would also like to thank Emrys Phillips and Jon Lee for their useful comments and two anonymous reviewers for helpful suggestions to improve the manuscript. Finally, we would particularly like to thank Ian Fairchild who, as well as initially suggesting Norfolk as a suitable area to test the technique, has given invaluable advice, feedback and encouragement at every stage of the work.

References

Alley, R.B., Blankenship, D.D., Bentley, C.R., Rooney, S.T., 1986. Deformation of till beneath ice stream B, West Antarctica. Nature 322, 57–59.
Alley, R.B., Blankenship, D.D., Bentley, C.R., Rooney, S.T., 1987. Till beneath ice Streams B. 3. Till deformation: evidence and implications. Journal of Geophysical Research 92, 8921–8929.
Alsop, G.I., Holdsworth, R.E., 2004. The geometry and topology of natural sheath folds: a new tool for structural analysis. Journal of Structural Geology 26, 1561–1589.
Alsop, G.I., Holdsworth, R.E., McCaffrey, K.J.W., 2007. Scale invariant sheath folds in salt, sediments and shear zones. Journal of Structural Geology 29, 1585–1604.
Archanjo, C.J., Silva, M.G., Castro, J.C., Launeau, P., Trindade, R.I.F., Macedo, J.W.P., 2006. AMS and grain shape fabric of the Late Palaeozoic diamictites of the Southeastern Parana Basin, Brazil. Journal of Geological Society 163, 95.
Arnaud, E., Eyles, C.H., 2002. Catastrophic mass failure of a Neoproterozoic glacially influenced continental margin, the Great Breccia, Port Askaig Formation, Scotland. Sedimentary Geology 151, 313–333.
Banham, P.H., 1965. Pleistocene deposits at Weybourne: new data. Proceedings of the Geologists' Association 76, 77–78.
Banham, P.H., 1968. A preliminary note on the Pleistocene stratigraphy of north-east Norfolk. Proceedings of the Geologists' Association 79, 469–547.
Banham, P.H., 1975. Glacitectonic structures: a general discussion with particular reference to the contorted drift of Norfolk. In: Wright, A.E., Moseley, F. (Eds.),Ice Ages: Ancient and Modern. Seel House Press, Liverpool, pp. 69–94.
Banham, P.H., 1977. Glacitectonites in till stratigraphy. Boreas 6, 101–105.
Banham, P.H., 1988. Polyphase glaciotectonic deformation in the contorted drift of Norfolk. In: Croot, D.G. (Ed.), Glaciotectonics; Forms and Processes. Balkema, Rotterdam, pp. 27–32.
Banham, P.H., Gibbard, P.L., Lunkka, J.P., Parfitt, S.A., Preece, R.C., Turner, C., 2001. A critical assessment of 'a new glacial stratigraphy for Eastern England'. Quaternary Newsletter 93, 5–14.
Banham, P.H., Ranson, C.E., 1965. Structural study of the contorted drift and disturbed chalk at Weybourne, North Norfolk. Geological Magazine 102, 164–174.
Benediktsson, Í.Ö., Schomacker, A., Lokrantz, H., Ingólfsson, Ó., 2010. The 1890 surge end moraine at Eyjabakkajökull, Iceland: a re-assessment of a classic glaciotectonic locality. Quaternary Science Reviews 29, 484–506.
Benn, D.I., 1995. Fabric signature of subglacial till deformation, Breidamerkurjökull, Iceland. Sedimentology 42, 735–747.
Benn, D.I., Evans, D.J.A., 2010. Glaciers and Glaciation, second ed. Hodder Education, London.
Bennett, M.R., 2001. The morphology, structural evolution and significance of push moraines. Earth-Science Reviews 53, 197–236.
Bennett, M.R., Waller, R.I., Glasser, N.F., Hambrey, M.J., Huddart, D., 1999. Glacigenic clast fabrics: genetic fingerprint or wishful thinking? Journal of Quaternary Science 14, 125–135.
Borradaile, G.J., Henry, B., 1997. Tectonic applications of magnetic susceptibility and its anisotropy. Earth-Science Reviews 42, 49–93.
Borradaile, G.J., Jackson, M., 2004. Anisotropy of magnetic susceptibility (AMS): magnetic petrofabrics of deformed rocks. Magnetic Fabric: Methods and Applications 238, 299–360.
Borradaile, G.J., Tarling, D.H., 1981. The influence of deformation mechanisms on magnetic fabrics in weakly deformed rocks. Tectonophysics 77, 151–168.
Boulton, G., Hagdorn, M., 2006. Glaciology of the British Isles ice sheet during the last glacial cycle: form, flow, streams and lobes. Quaternary Science Reviews 25, 3359–3390.
Boulton, G.S., 1986. A paradigm shift in glaciology? Nature 322, 18.
Boulton, G.S., Dobbie, K.E., Zatsepin, S., 2001. Sediment deformation beneath glaciers and its coupling to the subglacial hydraulic system. Quaternary International 86, 3–28.
Boulton, G.S., Hindmarsh, R.C.A., 1987. Sediment deformation beneath glaciers: rheology and geological consequences. Journal of Geophysical Research 92, 9059–9082.
Bowen, D.Q., Rose, J., McCabe, A.M., Sutherland, D.G., 1986. Correlation of quaternary glaciations in England, Ireland, Scotland and Wales. Quaternary Science Reviews 5, 299–340.
Butler, R.F., 1992. Paleomagnetism: Magnetic Domains to Geologic Terranes. Blackwell Scientific Publications, Boston.
Cifelli, F., Mattei, M., Chadima, M., Hirt, A.M., Hansen, A., 2005. The origin of tectonic lineation in extensional basins: combined neutron texture and magnetic analyses on undeformed clays. Earth and Planetary Science Letters 235, 62–78.
Cifelli, F., Mattei, M., Chadima, M., Lenser, S., Hirt, A.M., 2009. The magnetic fabric in undeformed clays: AMS and neutron texture analyses from the Rif Chain (Morocco). Tectonophysics 466, 79–88.
Clark, P.U., 1994. Unstable behavior of the Laurentide ice sheet over deforming sediment and its implications for climate change. Quaternary Research 41, 19–25.

Dunlop, D.J., Ozdemir, O., 1997. Rock Magnetism: Fundamentals and Frontiers. Cambridge University Press, Cambridge.
Evans, D.J.A., Hiemstra, J.F., 2005. Till deposition by glacier submarginal, incremental thickening. Earth Surface Processes and Landforms 30, 1633–1662.
Eyles, N., Day, T.E., Gavican, A., 1987. Depositional controls on the magnetic characteristics of lodgement tills and other glacial diamict facies. Canadian Journal of Earth Sciences 34, 2436–2458.
Eyles, N., Eyles, C.H., McCabe, A.M., 1989. Sedimentation in an ice-contact subaqueous setting: the mid-Pleistocene 'North Sea Drifts' of Norfolk. U.K. Quaternary Science Reviews 8, 57–74.
Eyles, N., Kocsis, S., 1988. Sedimentology and clast fabric of subaerial debris flow facies in a glacially influenced alluvial fan. Sedimentary Geology 59, 15–28.
Fish, P.R., Whiteman, C.A., 2001. Chalk micropalaeontology and the provenancing of middle Pleistocene Lowestoft Formation till in eastern England. Earth Surface Processes and Landforms 26, 953–970.
Fuller, M.D., 1962. A magnetic fabric in till. Geological Magazine 99, 233–237.
Gentoso, M.J., Evenson, E.B., Kodama, K.P., Iverson, N.R., Alley, R.B., Berti, C., Kozlowski, A., 2012. Exploring till bed kinematics using AMS magnetic fabrics and pebble fabrics: the Weedsport drumlin field, New York State, USA. Boreas 41, 31–41.
Gibbard, P.L., Clark, C.D., 2011. Chapter 7 – Pleistocene glaciation limits in Great Britain. In: Ehlers, J., Gibbard, P.L., Hughes, P.D. (Eds.), Quaternary Glaciations-Extent and Chronology: A Closer Look. Developments in Quaternary Science, pp. 75–93.
Goodsell, B., Hambrey, M.J., Glasser, N.F., 2002. Formation of band ogives and associated structures at Bas Glacier d'Arolla, Valais, Switzerland. Journal of Glaciology 48, 287–300.
Hamblin, R.J.O., 2000. A new glacial stratigraphy for Eastern England. Mercian Geologist 15, 19–62.
Hamblin, R.J.O., Moorlock, B.S.P., Rose, J., Lee, J.R., Riding, J.B., Booth, S.J., Pawley, S.M., 2005. Revised pre-Devensian glacial stratigraphy in Norfolk, England, based on mapping and till provenance. Netherlands Journal of Geosciences 84, 77–85.
Hambrey, J.M., Glasser, N.F., 2003. Glacial sediments: processes, environments and facies. In: Middleton, G.V. (Ed.), Encyclopedia of Sediments and Sedimentary Rocks. Kluwer, Dordrecht, pp. 316–331.
Hambrey, M., Huddart, D., Bennett, M., Glasser, N., 1997. Genesis of 'hummocky moraines' by thrusting in glacier ice: evidence from Svalbard and Britain. Journal of the Geological Society 154, 623.
Hambrey, M.J., Huddart, D., 1995. Englacial and proglacial glaciotectonic processes at the snout of a thermally complex glacier in Svalbard. Journal of Quaternary Science 10, 313–326.
Hart, J.K., 1990. Proglacial glaciotectonic deformation and the origin of the Cromer Ridge push moraine complex, North Norfolk, England. Boreas 19, 165–180.
Hart, J.K., 2007. An investigation of subglacial shear zone processes from Weybourne, Norfolk, UK. Quaternary Science Reviews 26, 2354–2374.
Hart, J.K., Boulton, G.S., 1991. The interrelation of glaciotectonic and glaciodepositional processes within the glacial environment. Quaternary Science Reviews 10, 335–350.
Hart, J.K., Roberts, D.H., 1994. Criteria to distinguish between subglacial glaciotectonic and glaciomarine sedimentation. I. Deformation styles and sedimentology. Sedimentary Geology 91, 191–213.
Hart, J.K., Rose, J., 2001. Approaches to the study of glacier bed deformation. Quaternary International 86, 45–58.
Hart, J.K., Rose, K.C., Martinez, K., 2011. Subglacial till behaviour derived from in situ wireless multi-sensor subglacial probes: rheology, hydro-mechanical interactions and till formation. Quaternary Science Reviews 30, 234–247.
Hiemstra, J.F., Zaniewski, K., Powell, R.D., Cowan, E.A., 2004. Strain signatures of fjord sediment sliding: micro-scale examples from Yakutat Bay and Glacier Bay, Alaska, U.S.A. Journal of Sedimentary Research 74, 760–769.
Hooyer, T.S., Iverson, N.R., Lagroix, F., Thomason, J.F., 2008. Magnetic fabric of sheared till: a strain indicator for evaluating the bed deformation model of glacier flow. Journal of Geophysical Research 113, 1–15.
Hopkinson, J., 1890. Magnetic properties of alloys of nickel and iron. Proceedings of the Royal Society of London 48, 1–13.
Hubbard, A., Bradwell, T., Golledge, N., Hall, A., Patton, H., Sugden, D., Cooper, R., Stoker, M., 2009. Dynamic cycles, ice streams and their impact on the extent, chronology and deglaciation of the British–Irish ice sheet. Quaternary Science Reviews 28, 758–776.
Huddart, D., Hambrey, J.M., 1996. Sedimentary and tectonic development of a high-arctic, thrust-moraine complex: Comfortlessbreen, Svalbard. Boreas 25, 227–243.
Iverson, N.R., Cohen, D., Hooyer, T.S., Fischer, U.H., Jackson, M., Moore, P.L., Lappegard, G., Kohler, J., 2003. Effects of basal debris on glacier flow. Science 301, 81–84.
Iverson, N.R., Hooyer, T.S., Thomason, J.F., Graesch, M., Shumway, J.R., 2008. The experimental basis for interpreting particle and magnetic fabrics of sheared till. Earth Surface Processes and Landforms 33, 627–645.
Jeffery, G.B., 1922. The motion of ellipsoidal particles immersed in a viscous fluid. Proceedings of the Royal Society of London. Series A, Containing Papers of a Mathematical and Physical Character 102, 161–179.
Jelínek, V., 1981. Characterization of the magnetic fabric of rocks. Tectonophysics 79, T63–T67.
Kazi, A., 1972. Clay mineralogy of the North Sea Drift. Nature 240, 61–62.
Khan, M.A., 1962. The anisotropy of magnetic susceptibility of some igneous and metamorphic rocks. Journal of Geophysical Research 67, 2873–2885.
Kissel, C., Barrier, E., Laj, C., Lee, T.Q., 1986. Magnetic fabric in undeformed marine clays from compressional zones. Tectonics 5, 769–781.
Kluiving, S.J., Rappol, M., Wateren, D.v.d., 1991. Till stratigraphy and ice movements in eastern Overijssel, The Netherlands. Boreas 20, 193–205.
Kurtz, D.D., Anderson, J.B., 1979. Recognition and sedimentologic description of recent debris flow deposits from the Ross and Weddell seas, Antarctica. Journal of Sedimentary Research 49, 1159–1169.
Lee, J.R., Phillips, E.R., 2008. Progressive soft sediment deformation within a subglacial shear zone – a hybrid mosaic-pervasive deformation model for Middle Pleistocene glaciotectonised sediments from eastern England. Quaternary Science Reviews 27, 1350–1362.
Lee, J.R., Rose, J., Hamblin, R.J.O., Moorlock, B.S.P., 2004. Dating the earliest lowland glaciation of eastern England: a pre-MIS 12 early Middle Pleistocene Happisburgh glaciation. Quaternary Science Reviews 23, 1551–1566.
Lee, J.R., Rose, J., Riding, J.B., Moorlock, B.S.P., Hamblin, R.J.O., 2002. Testing the case for a Middle Pleistocene Scandinavian glaciation in Eastern England: evidence for a Scottish ice source for tills within the Corton Formation of East Anglia, UK. Boreas 31, 345–355.
Lesemann, J.E., Alsop, G.I., Piotrowski, J.A., 2010. Incremental subglacial meltwater sediment deposition and deformation associated with repeated ice-bed decoupling: a case study from the Island of Funen, Denmark. Quaternary Science Reviews 3212–3229.
Licciardi, J.M., Clark, P.U., Jenson, J.W., Macayeal, D.R., 1998. Deglaciation of a soft-bedded Laurentide ice sheet. Quaternary Science Reviews 17, 427–448.
Lunkka, J.P., 1994. Sedimentation and lithostratigraphy of the North Sea Drift and Lowestoft Till Formations in the Coastal cliffs of northeast Norfolk, England. Journal of Quaternary Science 9, 209–2332.
MacAyeal, D.R., 1992. Irregular oscillations of the West Antarctic ice sheet. Nature 359, 29–32.
March, A., 1932. Mathematical theory on regulation according to the particle shape and affine deformation. Zeitschrift Fur Kristallographie 81, 285–297.
Mattei, M., Sagnotti, L., Faccenna, C., Funiciello, R., 1997. Magnetic fabric of weakly deformed clay-rich sediments in the Italian peninsula: relationship with compressional and extensional tectonics. Tectonophysics 271, 107–122.
McClay, K.R., Ellis, P.G., 1987. Geometries of extensional fault systems developed in model experiments. Geology 15, 341–344.
Menzies, J., van der Meer, J.J.M., Rose, J., 2006. Till as a glacial tectomict, its internal architecture, and the development of a typing method for till differentiation. Geomorphology 75, 172–200.
Moncrieff, A.C.M., 1989. Classification of poorly sorted sedimentary rocks. Sedimentary Geology 65, 191–194.
Nagata, T., 1961. Rock Magnetism. Maruzen, Tokyo.
Parés, J.M., van der Pluijm, B.A., 2002. Evaluating magnetic lineations (AMS) in deformed rocks. Tectonophysics 350, 283–298.
Perrin, R.M.S., Rose, J., Davies, H., 1979. The distribution, variation and origins of pre-Devensian Tills in Eastern England. Philosophical Transactions of the Royal Society of London. Series B, Biological Sciences 287, 535–570.
Phillips, E.R., Auton, C.A., 2000. Micromorphological evidence for polyphase deformation of glaciolacustrine sediments from Strathspey, Scotland. In: Maltman, A.J., Hubbard, B., Hambrey, J.M. (Eds.), Deformation of Glacial Materials. Geological Society London Special Publications, pp. 279–292.
Phillips, E.R., Lee, J.R., Burke, H., 2008. Progressive proglacial to subglacial deformation and syntectonic sedimentation at the margins of the mid-Pleistocene British ice sheet: evidence from north Norfolk, UK. Quaternary Science Reviews 27, 1848–1871.
Phillips, E.R., Merritt, J., Auton, C., Golledge, N., 2007. Microstructures in subglacial and proglacial sediments: understanding faults, folds and fabrics, and the influence of water on the style of deformation. Quaternary Science Reviews 26, 1499–1528.
Phillips, E.R., van der Meer, J.J.M., Ferguson, A., 2011. A new 'microstructural mapping' methodology for the identification, analysis and interpretation of polyphase deformation within subglacial sediments. Quaternary Science Reviews 30, 2570–2596.
Piotrowski, J.A., Larsen, N.K., Junge, F.W., 2004. Reflections on soft subglacial beds as a mosaic of deforming and stable spots. Quaternary Science Reviews 23, 993–1000.
Piotrowski, J.A., Mickelson, D.M., Tulaczyk, S., Krzyszkowski, D., Junge, F.W., 2001. Were deforming subglacial beds beneath past ice sheets really widespread? Quaternary International 86, 139–150.
Preece, R.C., Parfitt, S.A., Coope, G.R., Penkman, K.E.H., Ponel, P., Whittaker, J.E., 2009. Biostratigraphic and aminostratigraphic constraints on the age of the Middle Pleistocene glacial succession in north Norfolk, UK. Journal of Quaternary Science 24, 557–580.
Rees, A.I., Woodall, W.A., 1975. The magnetic fabric of some laboratory-deposited sediments. Earth and Planetary Science Letters 25, 121–130.
Richter, C., van der Pluijm, B.A., 1994. Separation of paramagnetic and ferrimagnetic susceptibilities using low temperature magnetic susceptibilities and comparison with high field methods. Physics of the Earth and Planetary Interiors 82, 113–123.
Riedel, W., 1929. Zur Mechanik geologischer Brucherscheinungen. Zentralblatt für Geologie und Paleontologie B, 354–368.
Roberts, D.H., Hart, J.K., 2005. The deforming bed characteristics of a stratified till assemblage in north East Anglia, UK: investigating controls on sediment rheology and strain signatures. Quaternary Science Reviews 24, 123–140.
Rochette, P., 1987. Magnetic susceptibility of the rock matrix related to magnetic fabric studies. Journal of Structural Geology 9, 1015–1020.

Rose, J., Moorlock, B.S.P., Hamblin, R.J.O., 2001. Pre-Anglian fluvial and coastal deposits in Eastern England: lithostratigraphy and palaeoenvironments. Quaternary International 79, 5–22.
Scheib, A.J., Lee, J.R., Breward, N., Riding, J.B., 2011. Reconstructing flow paths of the Middle Pleistocene British ice sheet in central-eastern England: the application of regional soil geochemical data. Proceedings of the Geologists' Association 122, 432–444.
Schwehr, K., Tauxe, L., 2003. Characterization of soft-sediment deformation: detection of cryptoslumps using magnetic methods. Geology 31, 203–206.
Shumway, J.R., Iverson, N.R., 2009. Magnetic fabrics of the Douglas Till of the Superior lobe: exploring bed-deformation kinematics. Quaternary Science Reviews 28, 107–119.
Slater, G., 1926. Glacial tectonics as reflected in disturbed drift deposits. Proceedings of the Geologists' Association 37, 392–440.
Smith, J.V., 2000. Flow pattern within a Permian submarine slump recorded by oblique folds and deformed fossils, Ulladulla, south-eastern Australia. Sedimentology 47, 357–366.
Stewart, R.A., Bryant, D., Sweat, M.J., 1988. Nature and origin of corrugated ground moraine of the Des Moines lobe, Story County, Iowa. Geomorphology 1, 111–130.
Stupavsky, M., Gravenor, C.P., 1975. Magnetic fabric around boulders in till. Bulletin of the Geological Society of America 86, 1534–1536.
Stupavsky, M., Gravenor, C.P., Symons, D.T.A., 1974a. Paleomagnetism and magnetic fabric of the Leaside and Sunnybrook Tills near Toronto, Ontario. Bulletin of the Geological Society of America 85, 1233–1236.
Stupavsky, M., Symons, D.T.A., Gravenor, C.P., 1974b. Paleomagnetism of the Port Stanley Till, Ontario. Geological Society of America Bulletin 85, 141–144.
Tarling, D.H., Hrouda, F., 1993. The Magnetic Anisotropy of Rocks. Chapman & Hall, London.
Thomason, J.F., Iverson, N.R., 2006. Microfabric and microshear evolution in deformed till. Quaternary Science Reviews 25, 1027–1038.
Thomason, J.F., Iverson, N.R., 2009. Deformation of the Batestown Till of the Lake Michigan lobe, Laurentide ice sheet. Journal of Glaciology 55, 131–146.
Twiss, R.J., Moores, E.M., 1992. Structural Geology. WH Freeman, New York.
van der Meer, J.M., 1993. Microscopic evidence of subglacial deformation. Quaternary Science Reviews 12, 553–587.
van der Wateren, F.M., 1999. Structural geology and sedimentology of the Heiligenhafen Till section, Northern Germany. Quaternary Science Reviews 18, 1625–1639.
van der Wateren, F.M., 2002. Processes of glaciotectonism. In: Menzies, J. (Ed.), Modern and Past Glacial Environments. Butterworth-Heinemann, Oxford, pp. 417–443.
van der Wateren, F.M., Kluiving, S.J., Bartek, L.R., 2000. Kinematic indicators of subglacial shearing. In: Maltman, A., Hubbard, B., Hambrey, J.M. (Eds.), Deformation of Glacial Materials. Geological Society London Special Publications, pp. 259–291.
Waller, R.I., Phillips, E.R., Murton, J., Lee, J.R., Whiteman, C., 2011. Sand intraclasts as evidence of subglacial deformation of Middle Pleistocene permafrost, North Norfolk, UK. Quaternary Science Reviews 30, 3481–3500.
West, R.G., Donner, J.J., 1956. The glaciations of East Anglia and the East Midlands: a differentiation based on stone-orientation measurements of the tills. Quarterly Journal of the Geological Society 112, 69–91.
Zaniewski, K., van der Meer, J.J.M., 2005. Quantification of plasmic fabric through image analysis. Catena 63, 109–127.